CORE-SHELL TYPE NANOCRYSTALLINE FTO PHOTOANODES FOR DYE SENSITIZED SOLAR CELLS

A THESIS SUBMITTED TO
THE GRADUATE SCHOOL OF NATURAL AND APPLIED SCIENCES
OF
MIDDLE EAST TECHNICAL UNIVERSITY

BY

KEREM ÇAĞATAY İÇLİ

IN PARTIAL FULFILLMENT OF THE REQUIREMENTS
FOR
THE DEGREE OF MASTER OF SCIENCE
IN
THE DEPARTMENT OF MICRO AND NANOTECHNOLOGY

AUGUST 2010

Approval of the thesis:

CORE-SHELL TYPE NANOCRYSTALLINE FTO PHOTOANODES FOR DYE SENSITIZED SOLAR CELLS

submitted by **KEREM ÇAĞATAY İÇLİ** in partial fulfillment of the requirements for the degree of **Master of Science in Micro and Nanotechnology Department, Middle East Technical University** by,

Prof. Dr. Canan Özgen _____
Dean, Graduate School of **Natural and Applied Sciences**

Prof. Dr. Zuhal Küçükyavuz _____
Head of Department, **Micro and Nanotechnology**

Prof. Dr. Ahmet Macit Özenbaş _____
Supervisor, **Metallurgical and Materials Eng. Dept**., **METU**

Prof. Dr. Raşit Turan _____
Co-Supervisor, **Physics Dept., METU**

Examining Committee Members:

Prof. Dr. Mehmet Parlak _____
Physics Dept., METU

Prof. Dr. Ahmet Macit Özenbaş _____
Metallurgical and Materials Eng. Dept., METU

Prof. Dr. Raşit Turan _____
Physics Dept., METU

Assoc. Prof. Dr. Caner Durucan _____
Metallurgical and Materials Eng. Dept., METU

Assist. Prof. Dr. Burcu Akata Kurç _____
Micro and Nanotechnology Dept. METU

Date: 13 August 2010

I hereby declare that all information in this document has been obtained and presented in accordance with academic rules and ethical conduct. I also declare that, as required by these rules and conduct, I have fully cited and referenced all material and results that are not original to this work.

Name, Last name : Kerem Çağatay İçli

Signature :

ABSTRACT

CORE-SHELL TYPE NANOCRYSTALLINE FTO PHOTOANODES FOR DYE SENSITIZED SOLAR CELLS

İçli, Kerem Çağatay
M.Sc., Micro and Nanotechnology Program
Supervisor: Prof. Dr. A. Macit Özenbaş
Co-Supervisor: Prof. Dr. Raşit Turan

August 2010, 97 pages

Aim of this work is to construct dye sensitized solar cells employing core shell type nanocrystalline FTO/TiO_2 photoanodes. Fluorine doped tin dioxide (FTO) nanoparticles were synthesized under hydrothermal conditions. Homogeneously precipitated SnO_2 nanoparticles were dispersed in aqueous solutions containing NH_4F as fluorine source and heat treated at 180^oC for 24 hours. X-Ray analysis revealed that particles show rutile type cassiterite structure. Particles had 50 m^2/g specific surface area measured by BET. Particle size was around 15-20 nm verified by XRD, BET and SEM analysis. Electrical resistivity of the powders measured with four point probe technique was around 770 ohm.cm for an F/Sn atomic ratio of 5, which showed no further decrease upon increasing the fluorine content of solutions. Thick films were deposited by screen printing technique and SEM studies revealed that agglomeration was present in the films which decreased the visible light transmission measured by UV-Visible spectrophotometry. TiO_2 shell coating was deposited by hydrolysis of ammonium hexafluorotitanate and $TiCl_4$ aqueous solutions. Efficiency of FTO nanoparticles was enhanced upon surface treatment where best result was 4.61 % for cells treated with $TiCl_4$. Obtained photocurrent of 22.8 mA/cm^2 was considered to be very promising for the future work. Enhancement

in efficiency was mostly attributed to suppressed recombination of photoelectrons and it is concluded that improved efficiencies can be obtained after successful synthesis of FTO nanoparticles having lower resistivity values and deposition of homogeneous shell coatings.

Keywords: Fluorine doped tin dioxide, dye sensitized solar cell, core shell type nanocrystals

ÖZ

BOYAYLA UYARILMIŞ GÜNEŞ HÜCRELERİ İÇİN ÇEKİRDEK-KABUK TİPİ NANOKRİSTAL FTO FOTOANOTLAR

İçli, Kerem Çağatay

Y. Lisans, Mikro ve Nanoteknoloji Programı

Tez Yöneticisi: Prof. Dr. A. Macit Özenbaş

Ortak Tez Yöneticisi: Prof. Dr. Raşit Turan

Ağustos 2010, 97 sayfa

Bu çalışmanın amacı çekirdek-kabuk tipi nanokristal FTO/TiO_2 fotoanotlardan oluşan boyayla uyarılmış güneş hücreleri üretmektir. Flor katkılanmış kalay dioksit (FTO) nanoparçacıklar hidrotermal koşullar altında sentezlenmiştir. Homojen çöktürme ile üretilen SnO_2 nanoparçacıkları, flor kaynağı olarak NH_4F içeren sulu çözeltilerde dağıtılmış ve 180^oC sıcaklıkta 24 saat süreyle ısıl işleme tabi tutulmuştur. X-ışını analizleri sonucunda rutil tipi kasiterit yapısında SnO_2 parçacıkların elde edildiği görülmüştür. Parçacıkların yüzey alanı BET yöntemiyle 50 m^2/g olarak ölçülmüştür. X-ışını, BET ve SEM analizleri 15-20 nm boyutlarında parçacıklar göstermiştir. Tozların elektriksel özdirenci, F/Sn atomik oranı 5 olan çözeltiler için 770 ohm.cm olarak ölçülmüştür ve artan flor konsantrasyonu ile özdirencin değişmediği gözlenmiştir. Kalın filmler serigrafi yöntemi ile kaplanmış olup, SEM analizi yapıda topaklanmalar göstermiştir. Bu topaklanmalar UV-Vis spektrofotometresi ile belirlenen görünür ışık geçirgenliği değerlerini düşürücü etki yapmıştır. TiO_2 kabuk kaplamaları amonyum heksaflorotitanat ve titanyum tetraklorür içeren sulu çözeltilerin hidrolizi ile elde edilmiştir. Yüzey işlemi sonucunda FTO nanoparçacıkların hücre verimleri arttırılmıştır. Elde edilen en yüksek verim değeri titanyum tetraklorür ile muamele edilmiş filmlerde % 4.61

olarak ölçülmüştür. Elde edilen 22.8 mA/cm^2 değerindeki akım yoğunluğu gelecek çalışmalar için son derece ümit vericidir. Verim değerlerindeki artışlar, fotoelektronların yeniden birleşme kayıplarının azalmasına bağlanmıştır. Daha düşük özdirence sahip parçacıkların elde edilmesi ve homojenliği yüksek kaplamaların yapılması sonucunda, verimlerde daha fazla artışlar olacağı sonucuna varılmıştır.

Anahtar Sözcükler: Flor katkılanmış kalay oksit, boyayla uyarılmış güneş hücresi, çekirdek kabuk tipi nanokristaller

To My Family

ACKNOWLEDGMENTS

I am very grateful to my supervisor Prof. Dr. A. Macit Özenbaş for his guidance and support during this work, and his great attention and patience on me from beginning until the end of my graduation.

It is great pleasure to thank my co-supervisor Prof. Dr. Raşit Turan from Physics Department of METU.

I am very grateful to my laboratory colleagues Halil İbrahim Yavuz, Murat Güneş and Özge Acarbaş, for their support and friendship at every stage of this work and my graduation.

I am very grateful to METU Metallurgical and Materials Engineering Department for all the support provided during this study. I want to thank to METU Central Laboratory for their attention during BET and SEM analysis. I want to thank to Eren Seçkin from Metallurgical and Materials Engineering Department of ITU for characterizations of solar cells.

I am very grateful to KOSGEB and Dr. Hüsniye Yaroğlu Güler for their attention and financial support during the construction of solar cells.

This work was also supported by GÜNAM (Center for Solar Energy Research and Applications) at METU.

I want to thank to my family, for their great patience and intense support, not only during this work but at every stage of my life.

TABLE OF CONTENTS

LIST OF TABLES

TABLES

LIST OF FIGURES

FIGURES

CHAPTER 1

INTRODUCTION

World's energy demand has been growing enourmously for several years and it is becoming more important for the developing countries to reach energy resources as world's population grows. Most of the energy being currently used depends on fossil fuels like oil, coal and natural gas although it is very well known that these energy resources cause serious environmental problems like global climate change which is a result of CO_2 emissions during energy production. Another aspect of fossil resources is their limited existence on earth and economical issues related with growing costs and availability. Many developed countries have declared that they have middle term programs on the reduction of dependency on fossil fuels and replace conventional resources with renewable counter parts. Besides most popular renewable energy resources like wind, geothermal and biomass, solar energy seems to be the most viable choice from the aspects of availability and abundance. Two common ways of using solar irradiation to produce electricity are solar thermal systems using sunlight to heat water and photovoltaic systems which directly converts solar irradiation to electricity using photovoltaic effect. While solar thermal systems need intense sunlight and warm climates which limit their usage in sun rich regions, photovoltaic devices can operate under moderate sun light levels and in a large interval of medium temperature. However, relatively high cost of photovoltaic energy conversion using photovoltaic panels limits their usage in energy production through other renewable resources and it is a popular field of research to increase efficiency of the devices while decreasing the cost of photovoltaic panels [1].

Photovoltaic industry has been recently dominated by silicon based photovoltaic panels. Although principles of photovoltaic energy conversion has been known for a

century, it has been a recently popular energy conversion method. As more companies and silicon producers are entering the market, cost of photovoltaic energy production per watt has been decreased from 7.5 USD to 4 USD since 1990. But it is still away from fossil fuel energy production costs. The main issue related with the high cost is the solar grade silicon which requires sophisticated and energy intensive production methods. In order to overcome high cost of silicon technologies, thin film photovoltaics have been introduced which decrease the use of materials and energy costs. However best thin film solar panels are still less efficient than monocrystalline silicon solar cells.

Among most popular thin film technologies, dye densitized solar cells (DSSC) are very promising candidates from the point of view of low cost materials used and ease of fabrication techniques. Since their invention in 1991 by Michael Graetzel and Brian O'Regan, a lot of attention has been paid on these photovoltaic devices**.** First DSSC contructed by Graetzel and O'Regan achieved 7% conversion efficiency while it has been risen up to 11% after several works of different groups around the world [2].

When compared with conventional p-n junction solar cells where excitation, charge separation and conduction occur on a semiconductor matrix under a built-in electrical field, DSSC shows novel excitation, charge separation and electronic conduction mechanisms. The main difference is the absence of a built-in electrical field inside the cell. Charge separation occurs in the dye-metal oxide interface and electrons are transported through the mesoporous matrix to the current collector and finally counter electrode by diffusion [3].

Unique working mechanism of dye sensitized solar cells makes them attractive for many applications as they are not affected by light intensity and angle of incidence. They do not suffer from elevated working temperatures as conventional cells go under efficiency degradation. Transparency and different colors of dye sensitized solar cells find applications in many areas like energy harvesting windows and

architecture. However, best laboratory efficiencies of 11% and 6-7% module efficiencies are lower than best thin film solar cells. There is extensive research to increase efficiency values comparable to pn junction solar cells.

One of the most popular approach to enhance efficiency values of dye sensitized solar cells is to employ different anode materials rather than nanocrystalline TiO_2 which gives best performances to date. Application of different metal oxides like SnO_2, Nb_2O_3, ZnO, ZrO_2 has been conducted but they cannot compete with TiO_2 due to high recombination and decreased photocurrents and photovoltages of these materials. Besides other metal oxides, SnO_2 has taken more interest as it is a wide band gap material showing high electron mobilities and electron diffusion coefficients which is widely used as transparent and conducting oxide coatings. Electrical properties of tin dioxide can be tailored upon doping with elements like antimony and fluorine, increasing the conductivity of the coating while maintaining a high visible light transmission. However, cells employing SnO_2 suffers from high recombination rates resulting from high electron mobilities and shows inferior efficiencies compared to TiO_2 [4].

Core-shell type nanoparticles have been investigated recently, promising suppression of recombination reactions in dye sensitized solar cells by creating energy barriers between photoelectrons and holes inside the electrolyte. Modification of nanoparticles with very thin coatings results in a core and shell configuration, which is employed as the anode part of the cells. This approach has become more popular which also leads to usage of different sensitizers and dye molecules by altering the electrochemistry of the anode [5].

The aim of this work is to enhance efficiency of tin dioxide by doping with fluorine and constructing core shell type SnO_2-TiO_2 photoanodes. For this purpose tin dioxide nanoparticles have been synthesized by common sol-gel methods and fluorine doping was achieved under hydrothermal conditions giving fluorine doped tin dioxide nanoparticles. Obtained powders were deposited as thick films on glass

substrates by screen printing technique. Core shell type anodes were constructed by modifying the surface of synthesized powders with TiO_2 by hydrolysis of titanium precursors from aqueous solutions. After a literature survey in the next section, experimental details were given in chapter 3. Results of the characterizations of the morphological, optical and electrical properties of powders and films using scanning electron microscopy, XRD, UV-Vis and four point probe measurements have been given in chapter 4. Parameters of solar cells with comparison of the bare and surface modified core shell type photoanodes and commercial TiO_2 nanoparticles were given and discussed extensively in chapter 4 and chapter 5.

CHAPTER 2

LITERATURE SURVEY

2.1. Photovoltaic Energy Conversion

Photovoltaic effect, since first observed by Becquerel, is known for a century. Development of first solar modules was motivated by space research and satellite applications. Solar photovoltaic energy conversion is becoming more popular these days, as it has many advantages over other renewable sources or conventional energy producing systems based on fosil fuels.

- Solar photovoltaic systems contain no moving parts which makes it unnecessary to conduct maintenance works.
- Photovoltaic energy conversion is completely renewable and limitless.
- Photovoltaic materials used in panels have long service time and contain no hazardous pollutants.
- There is no health problems associated with photovoltaic energy conversion systems.
- Materials used in photovoltaic panels are abundant on earth like silicon.
- Photovoltaic systems can be used in remote locations which give them flexibility.
- Research and manufacturing of photovoltaics are supported by a lot of companies and academia which makes us expect more developments in this technology.
- There has been significant research and development activities on photovoltaic systems in the past 20 years and cost of solar electricity production has been decreasing drastically through the years [6].

Materials used in photovoltaic devices are mainly semiconductors such as silicon and germanium. Properties of semiconductor materials can be tailored upon doping with certain elements and creating junctions by combining these structures. Solar radiation incident on photovoltaic devices are absorbed by semiconductor itself and charge carriers like electrons or holes are created and separated to achieve a net current. Observed current and voltage on photovoltaics is primarily determined by available solar spectrum on earth.

2.1.1. Solar Irradiance and Spectrum

Electromagnetic radiation coming from sun or any light source is a flux of photons, massless particles carrying energy. Photons show wave-like behaviour and characterized by wavelength λ, carrying an energy E_λ associated to its wavelength by:

$$E_\lambda = \frac{hc}{\lambda}$$

Eq. [2.1]

where *h* is the Planck constant and *c* is the speed of light.

Energy supplied by sun can be estimated from its black-body radiation of its surface temperature around 5762 K. Although this energy is homogeneous and isotropic, due to the distance between earth and sun and atmospheric effects tailor available solar energy on earth.

Above the atmosphere solar radiation intensity is 1353 kW/m^2 which is called as air mass zero. Air mass is the measure of solar radiation distribution affected by the athmosphere and it is given by:

$$\text{Air Mass} = \frac{1}{\cos\theta}$$

Eq. [2.2]

where θ is the angle of incidence. Solar radiation on sea level is referred to as air mass 1.5 which corresponds to 1.0 kW/m^2. This value is the standart spectral power to compare different solar cells. Figure 2.1 shows energy coming from sun with different wavelength for appropriate intensities.

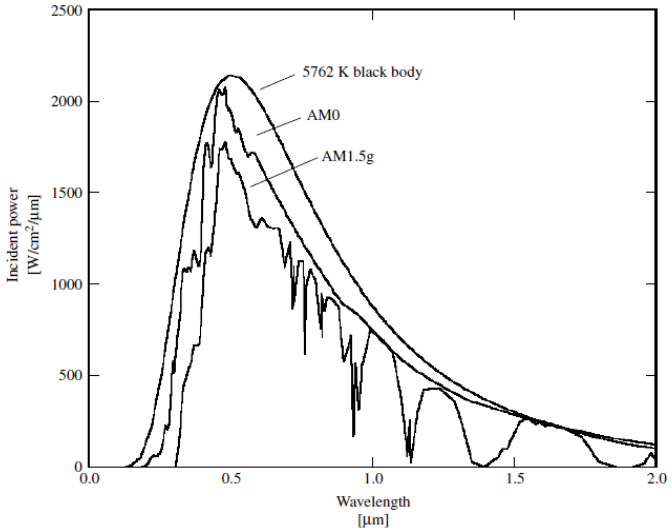

Figure 2.1 Solar Spectrum [6].

Energy available by sun incident on earth however can not be completely converted to energy. Conversion of this available energy depends on the nature and conversion mechanisms of solar cells and materials they are composed of.

2.1.2. Photovoltaic Devices and Semiconductors

Most photovoltaics are composed of materials called as semiconductor. These materials are intermediate materials between conductors and insulators. Term semi conductor arises from characteristic band gap and crystalline nature of these materials which give rise to unique properties. Semiconductors used in photovoltaic devices are mostly group IV of the periodic table or compounds of groups II and VI or III and V. These elements are summarized in Table 2.1.

Table 2.1 Semiconductor elements in periodic table.

I	II	III	IV	V	VI
		B	C	N	O
		Al	Si	P	S
Cu	Zn	Ga	Ge	As	Se
Ag	Cd	In	Sn	Sb	Te

Conventional solar cells are made from Si (group IV), GaAs (group III-V) and CdTe (group II-VI). Their characteristic band gaps determine the light absorption behaviour and transport kinetics. Band gap is a consequence of energy band structures of semiconductors. In general there is a forbidden gap in the electronic configuration of these materials which gives rise to separate valence and conduction bands. In their ground state, only valence band is occupied by electrons in normal temperature conditions. However upon illumination and absorption of light electrons can be excited to conduction band free to move across the crystal. Another way to create free carriers in semiconductors is to introduce impurity elements into the crystal lattice or as referred name doping of specific elements. Upon doping, band structure changes and new electronic states are present in the forbidden band called as donor or acceptor levels. These levels supply additional charge carriers like electrons in the case of donor states which is also called n type doping or so called holes in the case of acceptor states which is called as p type doping. Such doping can be achieved by introducing, for example, a group V element like phosphorus or antimony to a group IV element Si, which results in n type doping. Introducing a group III element like boron or aluminium to Si results in p type doping. A schematic diagram of these donor acceptor states are given in Figure 2.2.

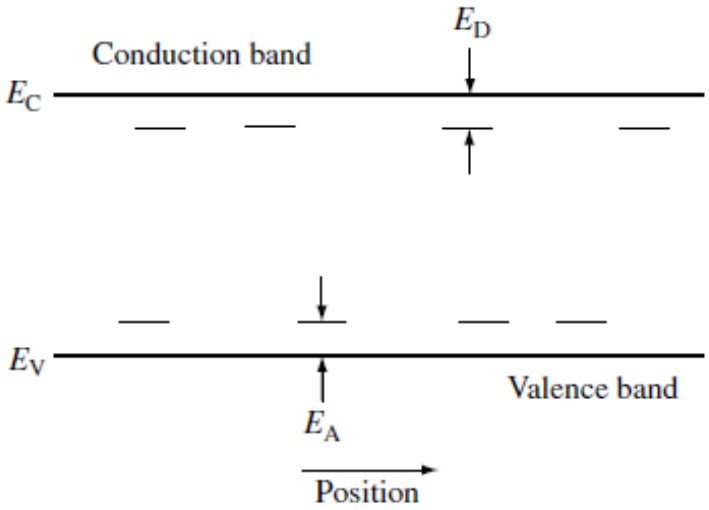

Figure 2.2 Donor and acceptor states in semiconductors [6].

In standart operating temperatures, thermal energy is sufficient enough to excite electrons or holes to conduction or valence band and these carriers are mobile which means free to move. However, this movement is random and there is no current flowing inside the semiconductor. Most interesting result occurs when an n type and p type semiconductor are brought together to form a metallurgical junction, called as pn junction.

2.1.3. pn Junction and Solar Cell

Figure 2.3 shows energy bands and electronic structure of a semiconductor when a p-type and n-type semiconductor is in contact to form a junction.

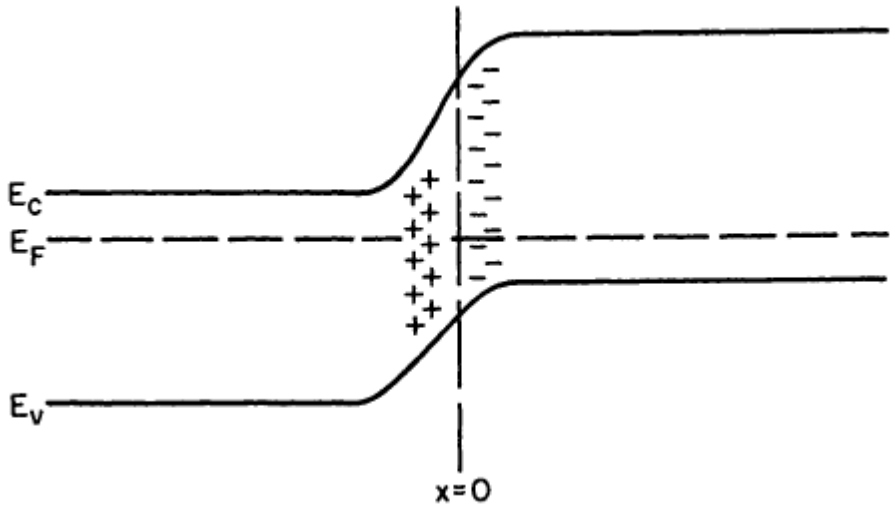

Figure 2.3 Energy bands in a pn junction [7].

The junction interface is the place where excess electrons and holes of the p-type and n-type semiconductors diffuse towards each other. This combination results in a net accumulation of positive and negative charges at the junction interface causing a built-in electrical field. Amount of this field determined primarily by the concentration of the dopants. As the fermi levels of the regions has to equilibrate, this field also gives rise to a rearrangement of band positions of the valence and conduction bands at the interface which is called as band bending. In this scheme electrons favors the n-type region and holes favor the p-type region separating the charge carriers. A typical solar cell is pn junction with a built in electrical field where electron hole pairs are separated from each other at this junction upon illumination and absorption of light.

2.1.4. Light Absorption in a Solar Cell

The basic working mechanism of a solar cell depends on the separation of electron hole pairs at the pn junction upon absorption of incident light. When a flux of photons are incident on a semiconductor three fundamental processes occur:

1. Reflection
2. Transmission
3. Absorption

Absorption of light by a semiconductor is a consequence of the capture of photons by an electron at valence band. If energy of the photon is larger than the band gap energy, then this electron is excited to the conduction band leaving an unoccupied place in the valence band, referred as a hole. Photons having lower energy than the gap energy are not absorbed but they are transmitted through the cell or they are reflected back from the surface.

In semiconductors, excitation of an electron from valence band to conduction band is referred as band to band transitions. From quantum physical point of view, such a transition has to fulfill the conservation of energy and also momentum rules. In direct semiconductors, where conduction band minimum energy has the same lattice momentum of maximum of valence band energy, such a transition occurs if a photon having sufficient energy is absorbed. However, in the case of indirect semiconductors, the transition requires also excess momentum so higher energy than the band gap is desirable. Sometimes it is also possible that lattice itself can provide this momentum from lattice vibrations or phonons, however these factors both decreases the chance of capturing a photon and results in lower absorption coefficients. For silicon, which has an indirect band gap, a thickness of nearly 200 microns is required unless optical confinement used, while much lower thicknesses can be sufficient for direct semiconductors like GaAs.

Besides band to band transitions upon light absorption, free carriers inside the cell can also absorb light called as free carrier absorption. This type of absorption occurs when conduction band electrons absorb light to excite higher energy levels inside the band. Band to band transition and free carrier absorption always happen simultaneously and free carrier absorption does not create electron hole pairs.

However, this type of absorption is significant only in high doping concentrations or under strong illumination [7].

2.1.5. Carrier Transport

In a typical pn junction, electrons and holes are in thermal equilibrium under steady state conditions. When light is incident on the junction, electron hole pairs or charge carriers are generated. These carriers are separated from each other under the internal electrical field so only electronic excitations occuring in the junction can contribute to the net electrical current. These electrons and holes which contribute to the current, can be expressed by the transport equations where current densities *J* are given by:

$$J_n = q\mu_n n\varepsilon + q.D_n\nabla_n$$

Eq. [2.3]

$$J_p = q\mu_p p\varepsilon - q.D_p\nabla_p$$

Eq. [2.4]

In these equations, current densities for both electrons and hole concentrations are defined by n and p, μ_n and μ_p electron and hole mobilities, D_n and D_p electron and hole diffusion coefficients, ε the electrical field and q is the elementary charge. First term of the equation describes the transport associated with the electrical field which is called as drift current and second part defines the transport with diffusion associated with the diffusion coefficient. This shows that main transport inside a pn junction is conducted by drift and diffusional effects. The diffusion coefficient and the mobility are the major factors affecting the transport directly. Although both parameters are characteristic properties of semiconductors and vary from material to material, there are several factors determining the both quantities. They are both affected by temperature, doping level and impurities inside the cell. These factors directly affects the performance of cells by certain mechanisms like lattice scattering,

impurity scattering, carrier-carrier scattering etc. These factors decreases the life time and diffusion length of electrons via recombination of photo generated charge carriers [8].

2.1.6. Recombination Losses

Recombination of charge carriers is another important parameter determining the efficiency of a solar cell. Photo generated carriers can recombine with each other through several processes, which are mostly categorized as bulk recombinations or surface state recombinations. Another characteristic of these recombinations may be distinguished from each other by radiative or non radiative recombinations. These recombinations can be summarized as:

- Band to band transitions
- Defect assisted recombinations (Trap levels)
- Auger recombination
- Recombination from surface states

Band to band transitions are the inverse process of light absorption. An electron capture from conduction band with a hole in the valence band results in emission of photon so they are radiative. In direct semiconductors this type of recombination is more significant than indirect semiconductors like silicon. Auger recombinations or the inverse auger may be radiative or non radiative where during a recombination process, excess energy of the electron is transmitted to another electron in the conduction band exciting that electron to higher energy levels. This excess energy is than emitted from the electron by phonon emission which is non radiative.

Most common and maybe the most important recombination is the defect assisted recombinations or recombinations via defect levels. These defect levels lie in the forbidden gap of the semiconductor close to the middle of the gap which do no contribute to acceptor or donor levels, also called as trap levels as illustrated in

Figure 2.4. These levels are created by either impurity atoms or defects in the lattice like dislocations or point defects. Recombination of an electron or a hole from these levels is mostly ends up with phonon emissions and non radiative. Rate of these recombination reactions is directly proportional to impurity concentrations so high purity semiconductor production is an essential from this point of view.

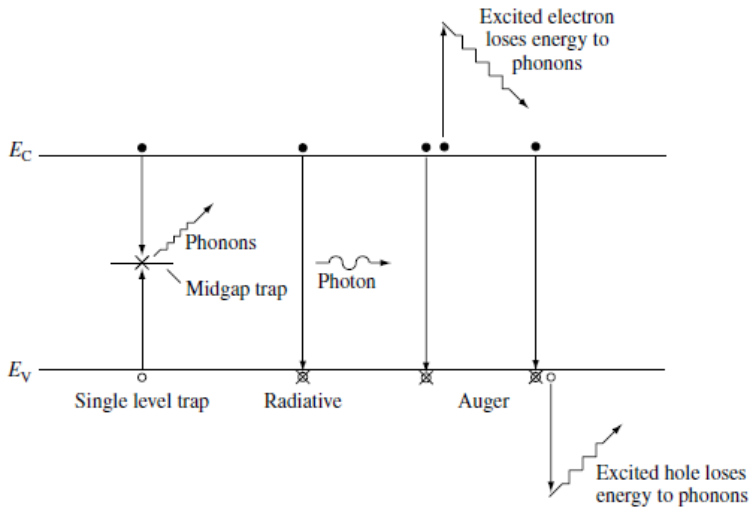

Figure 2.4 Recombination reactions in a semiconductor [6].

Surface recombinations rise from the fact that surfaces are quite different from bulk of the materials and as these regions contain dangling bonds and unbounded atoms, they have high defect concentrations. If carriers in the bulk reach these regions, high recombination rates can be observed. One way of preventing this type of recombination is the passivation of surfaces where dangling bond concentrations are lowered by bonding these regions to certain elements or using buffer layers. This technique is especially common in thin film solar cells where there is a high probability of carriers to reach surface regions [9].

2.2. Solar Cell Types

2.2.1. Crystalline Silicon Solar Cells

Photovoltaic industry is dominated by silicon solar cells occupying 85% of the market. Although other technologies are enourmously growing, microelectronic industry and supply of silicon is continuously pushing forward the silicon technologies. There are three types of silicon based solar cells.

1. Mono (Single) Crystalline Silicon
2. Multi (Poly) Crystalline Silicon
3. Amorphous Silicon

Crystalline type silicon is produced from molten silicon in the form of ingots, ribbons or wafers according to their crystal size which directly affects their performance. Because the main loss mechanism in these cells is defect recombination, purity and crystal size are the major factors determining both performance and cost of these materials. In order to obtain impurity free single crystalline silicon cells, Czochralski process is used where molten silicon and dopant atoms are solidified on a seed crystal by pulling the crystal under well controlled speed and temperature gradients. Ingots produced by this method contain impurities at very low concentrations and are single crsytalline. In the case of multicrystalline silicon, ingots are casted from molten silicon directly resulting a multicrystalline structure.

Because silicon has an indirect band gap of 1.17 eV, light absorption is relatively poor and for better optical response of the cells, thicker wafers have to be used between 200-300 microns, however diffusion length is lower than this thickness. Surface passivation reducing surface recombinations and surface texturing to enhance light absorption require many processes to be employed in industrial cells.

Starting from p type silicon wafers doped with boron, main production steps can be summarized as:

- Saw damage etching in alkaline or acidic solution
- Surface texturing to minimize reflection losses using NaOH
- Phosphorus diffusion for n type doping in quartz or belt furnaces
- Junction isolation
- Anti reflective coatings employing TiO_2 or SiN
- Printing front and back contacts using silver grids
- Firing of contacts
- Testing and characterization

Figure 2.5 shows the final structure of a typical silicon solar cell.

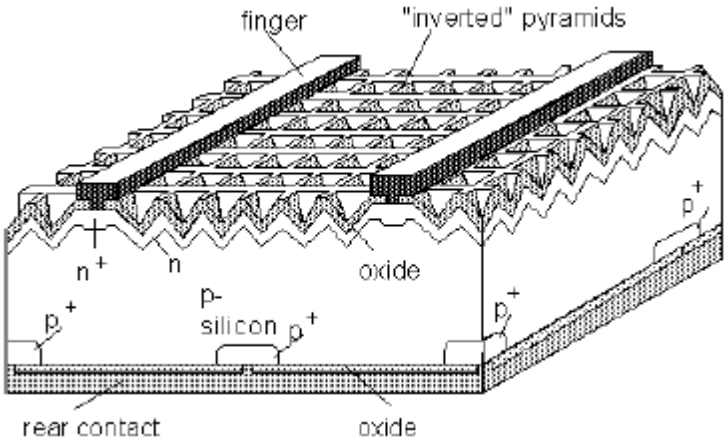

Figure 2.5. Typical crystalline silicon solar cell [10].

Best efficiencies of laboratory type crystalline cells has reached to 27%, close to its maximum theoretical limit while multicrystalline cells give around 20%. Commercial modules however have lower efficiencies than laboratory cells having efficiencies up to 18% and available from many manufacturers also varying from manufacturers according to manufacturing processes and technology used. In case of

crystalline cells, efficiencies change dramatically during real outdoor conditions due to variations in the temperature, light intensity and incidence angle during the day. Because of this reason actual performance of the commercial modules differs from standart test conditions and has to be determined for specific applications. Most of the companies give warranties up to 20 years for a service time [10].

2.2.2. Thin Film Silicon

Crystalline solar cells made of silicon in bulk have dominated the market for several years however, cost of these devices is a major problem for widespread use of photovoltaics. The cost of silicon material, as it is the major parameter leading to high cost of these devices, thin film approach is the most popular research topic for reducing panel costs. Many efforts have been spent on depositing thin silicon layers on substrates using techniques like evaporation, CVD, and liquid phase epitaxy. However, low absorption coefficient of silicon results in low light absorption and decreased efficiencies, today 16% has been achieved by light trapping techniques for thin film configurations.

Amorphous silicon is an alternative to crystalline silicon as thin film material as it has two orders higher absorption coefficient than crystalline silicon. However, amorphous structure leads to very high defect densities and recombination. Absence of long range order and only a few nanometers short range order results in dangling bonds and recombination centers. These unbound bonds can be passivated by introducing hydrogen into the structure. After doping, these recombination centers also increases again and pn junction formation is not possible with an effective charge collection so p-i-n configurations are used in these cells. In this configuration, an intrinsic silicon layer exists between the n-type and p-type silicon layers and act as major absorption layer where electrical field is created with the doped layers with an electrical field magnitude depending on doping amount. A wide range of techniques can be used to deposit amorphous silicon for different temperatures using silane (SiH_4) gas as the precursor by CVD techniques. Sputtering and plasma

enhanced CVD methods are also under investigation. Efficiencies around 10% has been achieved so far however these cells suffer from stability issues related to the breaking of Si-H bonds under illumination which can be regained after an annealing step [11].

2.2.3. Gallium Arsenide Solar Cells

GaAs is a popular group III-V compound widely used in semiconductor industry as an electronic and optoelectronic device. It has a band gap of 1.42 eV, close to optimum band gap value for solar cells. It has a direct band gap so light absorption for thin layers of this compound is very efficient. Junctions can be made by adding dopants like Al or Zn. Band gap of this compound can be tailored upon alloying or doping, so tandem devices can be created easily on the same substrate with common deposition methods. High tandem efficiencies can be obtained by using liquid phase epitaxy, MDVPE and molecular beam epitaxy. As long as GaAs is a very expensive material, GaAs substrates are subject to be replaced by other substrates like silicon or germanium, however thermal expansion mismatch is a problem. Besides being very expensive, both Ga and As are toxic materials and are avoided. Efficiencies as high as 26% have been achieved and they are widely used as panels in satellite applications [9].

2.2.4. Cadmium Telluride Solar Cells

CdTe has a direct band gap of 1.45 eV having the nearly optimum band gap value for solar cells without multijunctions. It belongs to II-VI groups of periodic table and referred as metal chalcogenides. It shows high absorption coefficient and p type conductivity. Mostly used superstrate configuration includes a p type CdTe layer in junction with n type CdS layer. The most attractive feature of CdTe cells is the simplicity of production and very high stability of the components due to very robust nature as a result of highly ionic bonding. It has excellent outdoor stability while space environment stability is superior to other technologies. Efficiencies up to 16%

has been reported and module efficiencies are around 10%. Although maximum theoretical limit of 29% has not been reached yet, further work on these cells are inhibited because of environmental issues related to cadmium. Deposition techniques vary according to process temperatures used where vacuum technologies like sputtering and high vacuum evaporation and other less expensive techniques like screen printing, spray pyrolysis, CVD and electrodeposition can be applied [11].

2.2.5. Copper (Indium, Gallium) Diselenide Solar Cells

Compounds semiconductors from the groups of I-III-V of periodic table are called as cholcopyrites having a tetragonal crystal structure. Electrical conductivity and band gaps of these compounds can be tailored by changing the stoichiometry of the compound. Mostly used elements are copper indium diselenide (CIS) or copper gallium diselenide. Their band gaps vary around 1.04 and 1.68 and mostly used high efficiency cells have around 1.20-1.25 eV. These structures have high absorption coefficient like CdTe and only a two micron thick layer is sufficient for an efficient light absorption. Cells contain a p type, slightly Cu deficient, $Cu(InGa)Se_2$ bulk structure where n type heterojunction is mostly CdS. CIGS cells produced with different techniques show similar performances which show that grain size effect is not a primary actor determining electronic conduction and recombination. Back contacts are made of molybdenum grown by sputtering and front contact material is a wide band gap TCO (Transparent Conducting Oxide), mostly ITO and ZnO. Many deposition techniques can be applied to deposit absorption layers like sputtering, evaporation techniques, electrodeposition, spray pyrolysis or printing. Efficiencies up to 19% have been achieved and module efficiencies are around 16% with several companies working to improve cost and efficiency of these cells [11].

2.3. Dye Sensitized Solar Cells (DSSC)

Dye Sensitized Solar Cells have been a great field of interest since their invention. The structure and working mechanism of dye sensitized solar cells distinguish them

from conventional photovoltaics where charge collection and separation is similar to plants. This similarity leads to a comparison with photosynthesis where in these cells the woring mechanism is called as artificial photosynthesis. Major components of dye sensitized solar cells as illustrated in Figure 2.6 are:

- Transparent and Conducting Glasses (TCO)
- Wide band gap semiconductor
- A monolayer of dye molecules attached on semiconductor matrix
- Redox electrolyte
- Catalyst coating on TCO

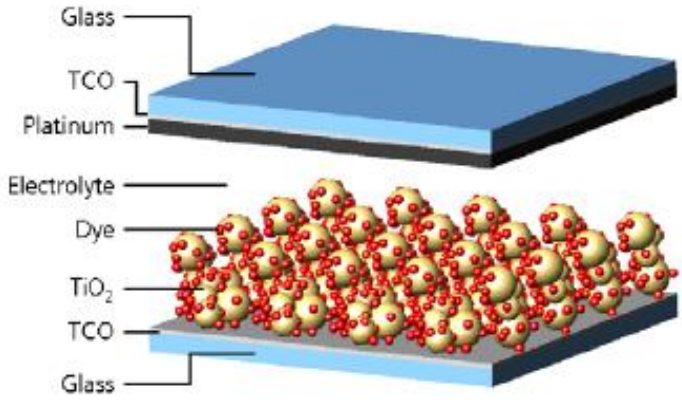

Figure 2.6 Structure of a dye sensitized solar cell [12].

Mainly, the anode of the cell is composed of a wide band gap (2.5-4 eV) metal oxide mesoporous structure. On the surface of nanoparticles of metal oxide, there is a monolayer of dye molecules absorbed on the surface sites of metal oxide. Dye molecule has a moderate energy difference between HOMO and LUMO states where photo-excitation occurs. The metal oxide is adhered to a conducting support which is mostly a transparent and conducting oxide like fluorine doped tin oxide or indium tin oxide, for an efficient charge collection. The counter electrode or the cathode of the cell is another transparent and conducting oxide on which a highly catalytic thin

layer exists like platinium or active carbon. A redox electrolyte is placed between the electrodes. The electrolyte consists of a redox couple which is mostly an iodide/triiodide couple and a solvent like acetonitrile or a non-volatile gel or ionic liquids. The cathode and the anode are brought together with an effective seal like hot melt polymers or glass frits and the whole cell is completed [13, 14].

2.3.1. Components of Dye-Sensitized Solar Cells

2.3.1.1. Transparent and Conducting Oxide (TCO)

Metal oxide to be used in dye sensitized solar cells are deposited on a transparent and conducting support, mostly fluorine doped tin oxide and indium tin oxide. The choice of TCO material arises from specific reqirements and process parameters during the construction of the cell. In general, TCO material to be employed is desired to have a low specific resistivity and high visible light transmission in the visible region of solar spectrum.

Basically, transparent and conducting oxides are polycrystalline, amorphous or exceptionally single crystalline materials which are mostly n type doped. In order to achieve high transparency, a wide band gap is desirable to prevent band to band electronic transitions by absorption of high energy photons, especially in the visible spectrum of solar radiation. However, wide band gap materials also behave like perfect insulators in their pure form. Electrical properties can be tailored upon doping with various dopants to the metal oxides as summarized in Table 2.2 which commonly results in n type doping although some exceptions exist where majority carriers are holes as it is for NiO. A typical transparent and conducting oxide shows resistivity values below 10^{-3} ohm.cm and high carrier densities above 10^{20} cm^{-3} [15].

Table 2.2 Semiconductors used in thin film TCOs [16].

Material	Dopant
SnO_2	Sb, F, As, Nb, Ta
In_2O_3	Sn, Ge, Mo, F, Ti, Zr, Hf, Nb, Ta, W, Te
ZnO	Al, Ga, B, In, Y, Sc, F, V, Si, Ge, Ti, Zr, Hf
CdO	In. Sn

Although best ITO films have better conductivity than FTO, the material of choice is not ITO because high temperatures up to 500^{o}C during the sintering of mesoporus anode causes high degrees of reduction in the conductivity of ITO. Commercially available FTO coatings on glass used in dye sensitized solar cells have sheet resistances of about 8-15 ohm/sq and a transmission of around 80% at 550 nm [16]. Besides ITO and FTO, there are numerous TCO materials to be employed in thin film photovoltaics like antimony doped tin oxide, aluminium doped zinc oxide, indium zinc oxide and etc.. Flexible TCOs of ITO on plastic substrates like PEN is also possible although they offer lower conductivity. Major contribution of TCO used in dye sensitized solar cells is the series resistance present inside the cell and the ohmic losses of photoinjected electrons. This problem is the key issue to enlarge laboratory type dye sensitized solar cells to commercial products. Chemical and mechanical stability is also another critical issue for dye sensitized solar cell applications where FTO has chemical inertness against most strong bases and acids and has a mohs hardness of 6.5 [16].

Most of the TCOs currently in use today are produced on glass substrates using expensive chemical vapour deposition or physical vapor deposition techniques like sputtering. However, there are several reports on producing transparent and

conducting oxide thin films using soft chemical routes like sol-gel or spray pyrolysis, which will cause strong reductions in the cost of dye sensitized solar cell [17].

2.3.1.2. Mesoporous Anode

The mesoporous anode or the photoelectrode is a high surface area and highly porous network of interconnected nanoparticles of wide band gap semiconductors, mostly metal oxides. The photoanode is the center of carrier generation, seperation and transportation. Most common metal oxides employed in dye sensitized solar cells are TiO_2, SnO_2, ZnO, Nb_2O_5, ZrO_2, but only anatase phase TiO_2 gives efficiencies of around 10%. Mesoporous and high surface area anode makes it possible to load large amounts of dye molecules absorbed on the sponge-like matrix. When compared to a flat 2-D layer of TiO_2, up to 15 microns thick layers of nanoparticle structures achieves up to 1000 times higher surface areas. Increase in the surface area results in higher amounts of dye molecules to be absorbed and chance of trapping an incident photon increases, which in turn results in a huge improvement of the photocurrent [18].

Another important characteristic of the anode is high porosity where liquid electrolyte can penetrate through with capillary action. The mesoporous network nanoparticles result in a porosity of 50-60% and behaves like sponge like structure as shown in Figure 2.7. This is important from a point of view of mass transport of electrolyte species which also limits the total current flowing inside the cell. Any counter effect suppressing the ionic transport also plays an important role in determining the photocurrent and also fill factor of the cell [18].

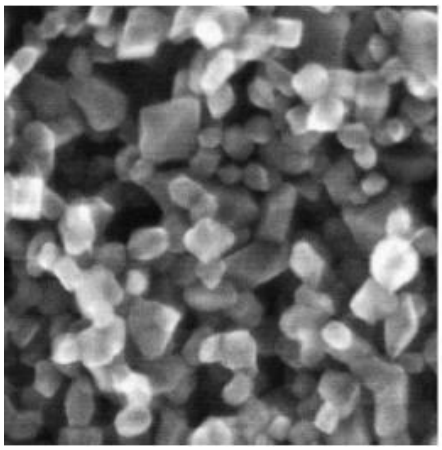

Figure 2.7 Mesoporous TiO_2 matrix [18].

In order to achieve desired properties of mesoporous metal oxide matrix, successful synthesis of nanoparticles and choice of deposition method is essential. Most metal oxides including anatase TiO_2 are synthesized by appropriate sol-gel techniques [19, 20].

Sol-gel chemistry of anatase titanium dioxide is based upon hydrolysis and condensation reactions of titanium precursors like titanium isopropoxide or titanium tetra chloride. Although there are several reports about application of commercially available TiO_2 nanopowders, nanoparticles with homogeneous distribution and desired optical and structural properties can be achieved by sol gel routes and following hydrothermal treatments.

It is well known that anatase phase of titanium dioxide is much more efficient than rutile phase so it is also desirable to obtain full anatase titanium dioxide [21]. The effect of preparation conditions and precursors used in the synthesis of titanium dioxide have been worked by several authors and it is reported that titanium dioxide nanoparticles hydrolized from aqueous $TiCl_4$ solutions give mixtures of anatase and rutile phases [22]. Most convenient way of making anatase titanium dioxide depends on hydrolysis of titanium isopropoxide and following treatments.

A typical synthesis prodecure of obtaining 20 nm diameter anatase titanium dioxide is as follows:

- Modification of titanium isopropoxide with acetic acid
- Hydrolysis with adding to water
- Peptization of titanium dioxide with nitric acid
- Filtering and washing with water
- Hydrothermal growth using autoclave at 250^{o}C
- Dispersion of nanoparticles with sonication
- Concentration of dispersion using evaporator [23]

Preparation of titania pastes includes dispersing the fine powders inside a vehicle and adding appropriate dispersion stabilizers or surfactants. Mostly used vehicles are viscous fluids like high molecular weight polyethylene glycol, carbowax, terpineol or water based dispersions including stabilizers to prevent agglomeration of particles and well dispersion like Triton-X100, tetramethylammonium hydroxide, ethylcellulose etc. Viscocity and concentration of the paste are the criticial issues to obtain crack free homogeneous layers of titanium dioxide. Non-homogeneous, aggregated or concentrated layers of titanium dioxide tends to peel of the substrate and results in failure of the coating [24].

Most convenient deposition method of metal oxides are tape casting, doctor blading or screen printing of the pastes. Each method has the advantage of using cheap and reproducible deposition conditions. After deposition of active layers, a following sintering process is unavoidable to ensure good interconnections between neighbouring particles and adhesion to the TCO substrate for efficient charge collection and transfer from mesoporous anode to external connections. Recently it has been shown that application of a thin titanium dioxide layer on the sintered anodes has a positive effect on the photovoltaic characteristics of the cells. Treatment of the anodes with $TiCl_4$ causes an increase in the surface roughness of the electrodes and increase dye uptake which results in higher photocurrents. Application of such

thin layers are also believed to increase interparticle connections and improve electron transport inside the mesoporous matrix. Performance of the cells are enhanced 10% upon $TiCl_4$ treatments [25].

Many reports have been published to replace nanoparticles with nanorods and nanotubes which promise efficient electron collection through the ordered anode instead of randomly connected nanoparticles. ZnO nanorods and TiO_2 nanotubes have been synthesized by several authors, however they are not sufficient enough to compete with 11% record efficiency of nanoparticle based anatase TiO_2 anodes up to date [26, 27].

2.3.1.3. Sensitizer

In dye sensitized solar cells, excitation of electrons by absorbed photons oocurs in sensitizer materials or in dye molecules. When considering the working mechanism of dye sensitized solar cells, the sensitizer dye is expected to absorb most of the solar spectrum and inject photoelectrons to the anode efficiently. As most of energy from sun comes in the visible region of solar spectrum, sensitizer should have a high incident photon to current efficiency in the range between 400-800 nm and it should have a high molar extinction coefficient which means a small portion of sensitizer should absorb all incoming light. For an efficient charge injection to metal oxide, energy of the excited state of the dye must lie above minimum of conduction band of the anode material [28]. Most dyes used in dye sensitized solar cells are organometallic complexes of ruthenium.

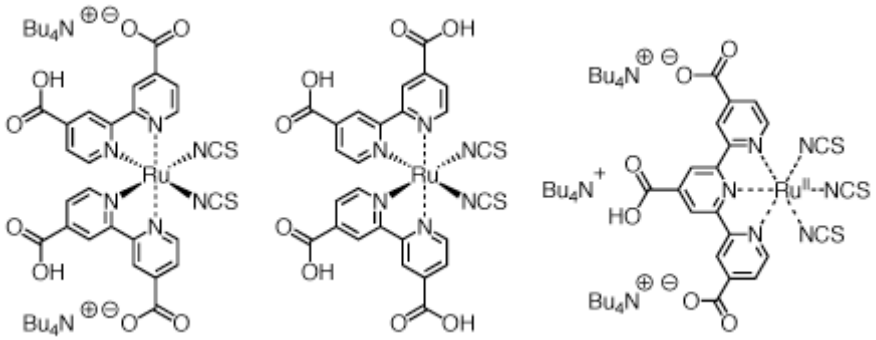

Figure 2.8 Structure of N719, N3 and black dye respectively [29].

Figure 2.8 shows different molecular structures of most popular ruthenium dyes. Adsorption process of dye molecules occurs through chemisorption where carboxyl groups attaches to TiO_2 surface and introduce one proton to lattice called as protonation. Excitation of electrons occurs from HOMO (highest occupied molecular orbital) of the dye molecule which is close to the metal atom, to the LUMO (lowest unoccupied molecular orbital) which is close to the bipyridine ligands. This configuration is believed to be the reason of ultrafast efficient charge transfer from molecular orbitals of the dye to TiO_2 conduction band. Another important parameter concerned with dye is the stability of these materials. It is desirable that dye molecules can achieve 10^8 oxidation reduction reactions which corresponds to 20 years life time. New and challenging issues related with sensitizers are the replacement of the expensive rare earth metal Ru with organic counter parts, application of quantum dots and tandem structures to shift response of the cell to IR region of solar spectrum [18].

2.3.1.4. Electrolyte

Electrolyte used in dye sensitized solar cells, which acts a hole conductor as analogous to pn junction cells, is the medium where reduction of dye cation is achieved and dye molecule is ready for the next excitation-injection reaction. For this purpose, the redox potential should lie above HOMO of the molecule but it should be below enough from the LUMO state and conduction band edge of the metal oxide for

a high photovoltage where maximum obtainable voltage is the difference between fermi level of electrons and the redox potential. Rate of reduction by the redox couple should be higher than reduction by conduction band electrons or excited state of the dye.

Most common electrolytes include I^-/I_3^- redox couple where iodide compounds like NaI, KI LiI up to 0.5 M with iodine I_2 up to 0.1 M are dissolved in solvents like acetonitrile, propionitrile, methoxypropionitrile or their mixtures. Viscosity of the solvent and mobilities of electrolyte species are very important for an efficient transport and electronic conductivity. In order to prevent a diffusion limited current during the operation of the cell, electrolyte species should have sufficient mobility and ionic conductivity inside the medium. Most solvents used in electrolytes are low viscosity low boiling point solvents. However this situation leads to another problem of stability of electrolyte under elevated temperatures which causes degradation of the cell and supressed life time. A lot of work has been done to replace volatile solvents with ionic liquids or gel electrolytes which resulted in improved stability of the cells although best efficiencies of these compounds are still inferior to those made with low viscosity electrolytes [30].

It is also desirable to develop transparent electrolytes besides iodide/triiodide couple in order to construct tandem structures. Because of high absorption of visible light by iodide, cells illuminated from back side show poor performance compared to front side illuminated ones.

2.3.1.5. Counter Electrode

Iodide ions oxidized to triiodide by reducing the dye cation are regenerated at the counter electrode by recombining with photoelectrons coming over the external load. Rate of this chemical reaction has to be very high and overpotentials which in turn lower the maximum photovoltage have to be prevented. For this purpose a catalyst is applied to counter electrode surface which is the interface between electrolyte and

conducting oxide glass. Most common catalyst is platinium where gold and carbon also can be applied. Coating can be deposited by sputtering or evaporation resulting films of up to 100 nm. Another method is to apply platinium precursors deposited by spraying or screen printing. From an economical point of view, platinium has to be replaced with carbon. Recent studies have shown that very high surface area carbon nanoparticles show comparable catalytic activity to platinium [31].

2.3.2. Working Mechanism

Figure 2.9 represents electron dynamics and electron energy levels present in a dye sensitized solar cell.

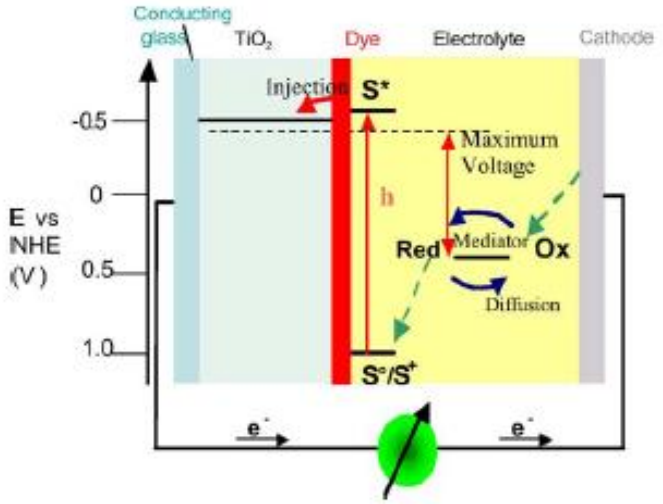

Figure 2.9 Electronic energy levels in a dye sensitized solar cell [18].

The photo excitation of electrons occurs in the dye molecules. Upon irradiation, an electron is excited from the highest occupied molecular orbital (HOMO) to the lowest unoccupied electron orbital (LUMO). This excited electron which is called the photoelectron, is then injected to the conduction band of the metal oxide. This process is known as the sensitization of metal oxide and occurs on the order a few picoseconds where following regeneration of dye molecule happens in a few nanoseconds. These injected photoelectrons are then transported through the metal

oxide mesoporous matrix to the TCO collector. The photoanode and the counter electrode are in contact through an external load where the electrons are transported while they make a net work on the load. The ionized dye molecule is re-oxidized by the redox couple present in the solution. Conversion of I^- to I_3^- occurs between dye and electrolyte interface and I_3^- molecules are transported to the counter electrode through the electrolyte with ionic diffusion mechanism. The electrolyte species are recombined with injected photoelectrons on the surface of counter electrode in the presence of the catalyst. This catalyst enhances the rate of redox reactions and is also responsible from the prevention of overpotentials at the counter electrode.

2.3.3. Electronic Transport and Recombination

Electron transport kinetics in dye sensitized solar cells differ much from conventional pn junction cells. Charges, in the manner of negatively charged electrons and positively charged holes, are separated in the dye metal oxide interface and transported by electron diffusion and ionic mass transport in electrolyte. In contrast to pn junction cells concepts like band bending and depletion layers are not present in dye sensitized solar cells, so many effort have been spent to understand electron dynamics and develop transport models. High surface area and roughness factor of mesoporous matrix make it impossible to explain photoelectrochemical characteristics of these cells using models to simulate planar semiconductors [32]. Most common techniques used to investigate the transport and recombination dynamics in dye sensitized solar cells are intensity modulated photovoltage and photocurrent spectroscopy, electrical impedance spectroscopy and transient photovoltage and photocurrent techniques. All these techniques measure response of the system to small or periodic perturbations. Using these tools, one can determine the characteristics which influence the electron transport and recombination and obtain quantitative data about the lifetime of photoelectrons, photovoltage dynamics, diffusion coefficient, electron charge inside the film, recombination time, spatial distribution of electrons under open and short circuit condition either under illumination and dark [33].

Basic electron transfers involved in a dye sensitized solar cell under illumination can be summarized as follows at short circuit conditions, D, D^+ and D^* are dye molecule, dye cation and exited state of dye, respectively, R and O is the redox species and e_{cb}^- and e_{pt}^- are conduction band electrons and electrons in the platinium layer, respectively.

$$D + hv \rightarrow D^* \qquad \text{Eq. [2.5]}$$

$$D^* \rightarrow D^+ + e_{cb}^- \qquad \text{Eq. [2.6]}$$

$$D^+ + R \rightarrow O \qquad \text{Eq. [2.7]}$$

$$O + e_{pt}^- \rightarrow R \qquad \text{Eq. [2.8]}$$

If there is an open circuit condition, electrons in the conduction band of metal oxide recombine with redox element or they directly recombine with dye molecule.

$$e_{cb}^- + O \rightarrow R \qquad \text{Eq. [2.9]}$$

$$e_{cb}^- + D^+ \rightarrow D \qquad \text{Eq. [2.10]}$$

The external quantum efficiency or incident photon to current efficiency (IPCE) is defined as the efficiency of each photon incident on a semiconductor to supply electron to current inside the cell.

By means of efficiency of electron absorption (η_{abs}), injection (η_{inj}) and collection (η_{coll}), IPCE can be defined as the product of each process:

$$\mathrm{IPCE} = \eta\eta_{abs} * \eta\eta_{inj} * \eta\eta_{coll} \qquad \text{Eq. [2.11]}$$

The back reaction of conduction band electrons inside the metal oxide matrix with electrolyte species or dye cations is also an important process under short circuit conditions and directly affects obtainable maximum value of IPCE and photovoltage. The observed photovoltage and photocurrent in dye sensitized solar cells primarily depend on the fact that interfacial recombination of conduction band electrons with redox electrolyte is considerably slower than reduction of redox species at the platinized counter electrode. As the concentration of photoelectrons increase in the conduction band, a useful photovoltage is obtained. These back reactions, also referred to as recombination, determine the diffusion length L_n of injected electrons which is defined as:

$$L_n = \sqrt{D_n.\tau_n}$$

Eq. [2.12]

Here, D_n is the diffusion coefficient and τ_n is the electron life time. Both parameters are not constant but depends on light intensity [34]. However, diffusion length itself is not affected by the intensity. As illumination increases diffusion coefficient increases but electron life time decreases. This phenomenon is attributed to multiple trapping of photoelectrons. Trapping and detrapping of electrons from trap states present inside the matrix leads to such behaviour. These traps act as recombination centers for electrons and are the result of nanoparticles and impurities inside the matrix. These trap states are distributed inside the network of nanoparticles and act as recombination centers. Trapping of electrons by the trap states inhibits photo current as only conduction band electrons are free to move. However these trapped electrons can be thermally re-excited to conduction band referred as detrapping with an associated waiting time. Reason of these trap states inside the band may originate from impurities or defects in the crystal. This type of behaviour is common in most amorphous or polycrystalline materials. Band tails inside the conduction band are believed to be a reason of surface states and show an exponential trap state distribution explaining the depence of light intensity on diffusion coefficient [33].

Transport of electrons inside the TiO_2 matrix is believed to ocur with ambipolar diffusion. As the electrolytes used in dye sensitized solar cells have very high ionic strength, diffusion of electrons during their transport is followed by cations inside the electrolyte and an internal electrical field is suppressed by the screening effect of these cations. This screening effect causes electroneutrality which is over a length scale, the Debye length about 0.1 nm as the electrolyte species can not penetrate to the bulk. This situation, to some extent, retards the electronic diffusion, however anionic species are also repelled from electrons so it enhances the ionic motion of negatively charged ions inside the electrolyte.

Electronic transport of electrons is highly affected by the film morphology. The performance difference between rutile and anatase phase TiO_2 is attributed to the morphological differences where rutile TiO_2 has less particle connections than anatase which suppresses electronic motion.

Interconnection of particles is quite important for efficient electronic transfer between particles. Coordination of neighbouring particles is mostly related with the porosity of the films. 75% porosity films have particles with a coordination number of 2.5 while 50% porosity causes a coordination number of 5. According to the random walk theory of electrons, diffusion coefficient is highly related with this porosity. Highly porous films cause electrons to travel longer pathways during transport although there are less particles per unit volume. Magnitude of diffusion coefficient in nanoparticle systems is much lower than single crystal TiO_2 due to the interparticle necking and porous structure, however this cannot explain the dependence of diffusion coefficient on light intensity. This dependence can be explained by the trapping-detrapping model of electrons [33].

Although the main mechanism of electronic transport is diffusion in the absence of a built in electrical field, electron distribution and concentration profiles may lead to electrical fields in microscale and contribute to transport in addition to diffusion. Difference between the diffusion coefficient of random walk process and the

observed effective coefficient is mostly attributed to this concentration gradient of electrochemical potential. Electronic concentration gradient is believed to cause band bending in conduction band and built in electrical fields. As this field can be neutralized by Helmholtz layer in the interface, at high intensities, it may significanly enhance the diffusion coefficient [35].

Recombination of photoelectrons in dye sensitized solar cells occurs very differently from conventional solar cells. As there exist no holes in TiO_2, recombination reactions and ways differ from pn junctions. Most of recombination reactions occur at the metal oxide-electrolyte interface and it is important to determine where exactly these reactions take place. Recombination time for electrons in dye sensitized solar cells depends on light intensity and this time may change from miliseconds to several seconds. The successful performance of dye sensitized solar cells rises from the fact that recombination reactions are much slower than transport of electrons and charge collection efficiencies are pretty high.

Possible recombination reactions are given in Figure 2.10. These reactions can be summarized as :

- Recombination of excited state of the dye with HOMO
- Recombination of conduction band photoelectrons with HOMO
- Recombination of conduction band electrons with redox couple

The most hazardous reaction of these processes is the recombination of photoelectrons with electrolyte. Rate of this reaction is the highest and it may occur at metal oxide or TCO electrolyte interface.

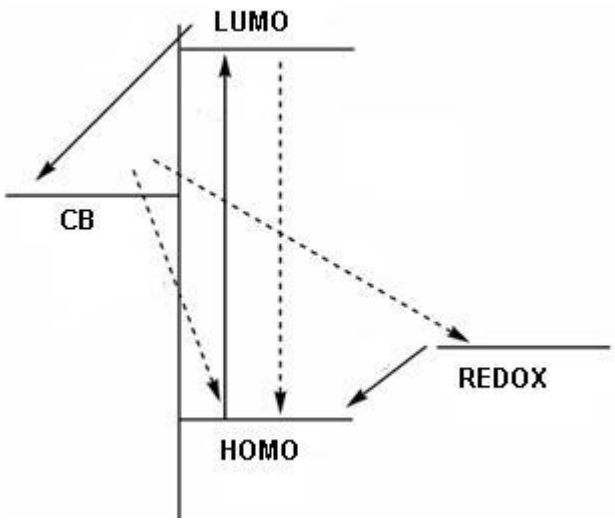

Figure 2.10 Possible recombination reactions in a dye solar cell.

Researches show that this reaction takes place primarily at the metal oxide electrolyte interface, however in dye sensitized solar cells with other redox couples than iodide/triiodide, recombination is faster at the TCO surface. Rate of this reaction also depends on diffusion coefficient. Factors inhibiting the diffusional transport of electrons also inhibit the rate of recombination which shows that rate of recombination is directly affected by diffusion of electrons [33].

2.4. Fluorine Doped Tin Dioxide

Tin dioxide is well known ceramic material used widely in industry. It belongs to a class of wide band gap semiconductors as many transition metal oxides. It is used as a gas sensing agent and oxidation catalyst. Another major field of application is transparent and conducting oxide material. High electronic conductivity and transparency in the visible region makes it a very suitable material for optoelectronic devices, especially doped tin dioxide [36] .

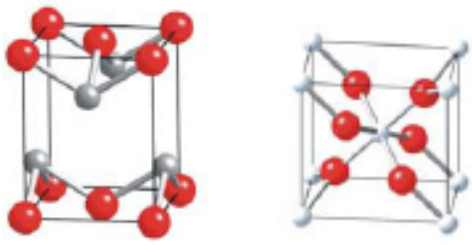

Figure 2.11 Crystal structures of tin oxide (litharge type) on the left and tin dioxide (rutile type) on the right [36].

Tin oxide has two major oxidation states with oxygen where +2 state also referred as stannous oxide (SnO) and tin dioxide has +4 state referred as stannic oxide (SnO_2). Stannic oxide is more abundant in earth rather than stannous oxide. Stannic oxide has the tetragonal rutile lattice structure while stannous oxide has the rare litharge structure. Stannous oxide has tetragonal lattice with constants a=b=3.8029 A and c= 4.8382 A where each Sn and O atoms are four fold coordinated. Stannic oxide also called cassiterite as the mineral name, shows rutile type structure with lattice constants of a=b=4.7374 A and c=3.1664 A where Sn atoms are six fold coordinated to three fold coordinated oxygen atoms as shown in Figure 2.11 [37]. Some physical properties of tin dioxide is given in Table 2.3.

Table 2.3 Selected physical properties of tin dioxide.

Property	**Tin Dioxide**
Mineral name	Cassiterite
Crystal structure	Tetragonal, rutile
Density (g/cm^3)	6.99
Mohs hardness	6.5
Melting point	$>1900^oC$
Band gap	3.6 eV

Tin dioxide has a wide fundamental band gap of around 3.6 eV and so it is transparent in the visible region of solar spectrum and at higher energies of solar radiation, the ultra violet region, band to band transitions from valence band to conduction band start and transparency decreases. Due to high gap between bands, it acts like an insulator in its pure form, however electrical properties of tin dioxide can be tailored upon doping with certain elements. Introduction of impurities alters the electronic structure of tin dioxide and create donor levels inside the gap as similar to other semiconductor materials. This fact makes this material a perfect candidate for possible optoelectronic applications where visible transparency and electrical conduction is required.

Improvement in electrical conduction of tin dioxide upon doping results from donor states inside the band gap. Impurity atoms introduced into lattice donate extra electrons to conduction. Amount of this donation depends on the concentration of donor atoms which are usually limited by the solubility of impurities in tin dioxide forming solid solutions. For the case of antimony, which has oxidation state of +5 in contrast to +4 state of tin atoms donates one extra electron where antimony may have an other oxidation state of +3 results in no donation [16].

Fluorine is another common dopant of tin dioxide has a valency of -1 where oxygen has -2 state. Fluorine atoms substitutionally replacing oxygen atoms donate one extra electron to conduction band and increase free carrier concentration. It is important that fluorine should replace oxygen substitutionally instead of placing into interstitial region inside lattice. Besides fluorine or antimony doping, lattice defects of oxygen are also another important electron donors. This type of donation is very important for ITO films where additional oxygen deficiencies are created in these films by reducing the material inside reducing atmospheres like hydrogen [38]. However, for the case of tin dioxide, it was shown that oxygen vacancies are less important by means of electron donation [37].

Increasing the free carrier concentration for electrical conduction in turn reduces the transparency of transparent and conducting oxides. High electron concentration in the conduction band results in free carrier absorption edge of electrons to lower wavelength values and near IR absorption of oxides starts to be significant [16].

Transparent and conducting films of fluorine doped tin dioxide can be deposited by several methods. Mostly used techniques are expensive CVD techniques giving homogeneous thin films. Plasma enhanced CVD and sputtering techniques are also applied [39]. Spray pyrolysis is another common technique to deposit thin continuous films using aqueous or alcoholic solutions of tin precursors. Best resistivity values obtained by this method are also comparable to films produced by CVD techniques [40, 41].

Nanoparticle based tin dioxide films are also deposited on glass substrates by common wet gel methods like dip coating or spin coating techniques [42]. These films are extensively used in gas sensors. However films of fluorine doped tin dioxide are very limited and give high resistivity values compared to CVD or spray pyrolized films. This situation is a result of high number of grain boundaries scattering conduction electrons and arises from the nanoparticulate nature. Because of this reason application of fluorine doped tin dioxide nanoparticles is very limited.

2.4.1. Application of Tin Dioxide in DSSC

Tin dioxide with high transparency and abundance is a suitable wide band gap semiconductor for dye sensitized solar cell applications. High electron mobilities and diffusion coefficient of electrons inside tin dioxide matrix are very attractive features where electronic transport of electrons are believed to occur efficiently as compared to TiO_2. However cells made from tin dioxide show very poor efficiencies compared to other metal oxides [43-50]. Efforts have been conducted to improve cell efficiencies by optimization of mesoporous matrix like synthesizing optimized

particles and improve electronic conduction and dye uptake. However, cells still could not compete with TiO_2 with a little change in efficiency [51].

Tin dioxide based cells show 200-300 mV less photovoltage compared to TiO_2 cells which are related to the more positive conduction band edge of SnO_2. Fermi level of electrons inside tin dioxide matrix lies below the fermi level of electrons in TiO_2 and observed photovoltage is lower [52]. Another important parameter is the more acidic character of SnO_2 surface which hinders dye absorption onto particle surface compared to other metal oxides which also lowers photocurrents [47].

Investigations showed that the main reason of performance of tin dioxide rises from the fact that increased mobilities of electrons inside the matrix also increases recombination rates simultaneously. High electronic mobility of electrons causes an increase in the chance of capture of photoelectrons by oxidized dye molecules or electrolyte species. Durrant et al showed in their extensive research that both electron transport and recombination dynamics are 2-3 orders faster than TiO_2 and slow carrier collection of TiO_2 based cells leads to decreased recombination. Although electronic mobility and diffusion coefficients are higher in SnO_2 cells, recombination is also high and electron lifetime is very short [53]. They conclude that application of barrier layers may be a key strategy to suppress electron recombinations and inhibit the electron loss inside the matrix. Table 2.4 gives a brief literature summary of tin dioxide based dye sensitized solar cells.

Table 2.4 Literature survey of SnO_2 based dye sensitized solar cells.

Reference	V_{oc} (V)	J_{sc} (mA/cm^2)	Fill Factor	Efficiency (%)
[43]	0.250	11.2	0.26	*0.74*
[44]	0.430	11	-	*2.6*
[45]	0.330	12	0.32	*1.3*
[46]	0.330	2.8	0.45	*0.5*
[47]	0.480	6.4	0.40	*1.2*
[48]	0.380	9.5	0.46	*1.66*
[49]	0.445	5.8	0.49	*1.26*
[50]	0.620	7.23	0.43	*2.63*

2.5. Core Shell Type Anodes

Studies of electronic transport and recombination dynamics on dye sensitized solar cells have revealed that electron losses due to recombination reactions mostly occur at the metal oxide electroyte interface. Control of electronic transitons at this interface is the major research of field of enhancing the charge collection and efficiency of the devices. Methods like modifying the uncoated places of particles and passivation of the active recombination sites have been employed by introducing agents into electrolyte [57]. A similar approach is application of barrier layers between particle electrolyte interface by coating the surface of particles with ultra thin layers of different compounds [45, 47, 54, 55, 56]. Such methods require the synthesis of core shell type particles with core material and thin shell coating. The main idea of this approach is to create energy barriers and decrease the recombination rates by suppressing the chance of capture of photoelectrons. Resulting structure is shown in Figure 2.12.

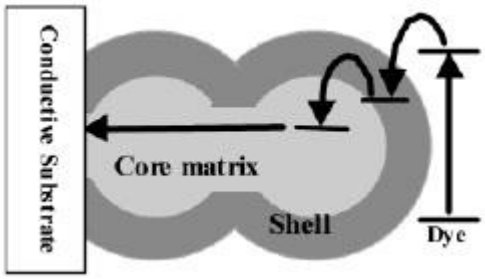

Figure 2.12 Core-shell structure of two metal oxides [52].

For electronic transitions between two layers to occur, electrons have to be driven from outer shell to the core so there has to be a chemical driving force for this process. Conduction band edge of the inner core should be more positive energy value than the shell where electrons will favor less energetic levels. Figure 2.13 shows conduction and valence band energies of various wide band gap semiconductors.

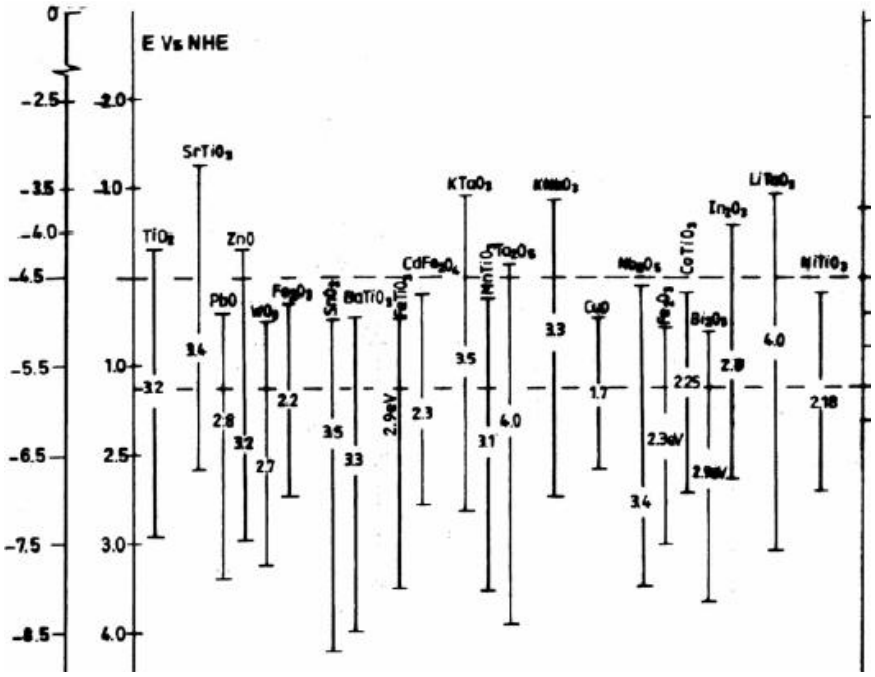

Figure 2.13 Conduction and valence band potentials of various semiconductors [7].

In this scheme, electronic coupling of LUMO energy of the dye and conduction band minimum of the outer shell are also important for an efficient electron transfer from dye to conduction band as high conduction band potential will suppress electron injection and decrease the photo current.

For the case of tin dioxide, choice of outer shell material is ZnO and TiO_2, which both have a conduction band potential of around 100 mV more negative than SnO_2. TiO_2 is a well known material which can be efficiently sensitized by the most common Ru dyes and can be deposited by various techniques easily on tin dioxide while rutile phase of TiO_2 matches well with the rutile type cassiterite structure of SnO_2.

Table 2.5 gives a brief summary of core shell type photoanodes investigated by researchers.

Table 2.5 Cell parameters of core shell type anodes employed in DSSCs.

Reference	Core	Shell	V_{oc} (V)	J_{sc} (mA/cm^2)	Fill Factor	Efficiency (%)
[45]	SnO_2	MgO	0.725	15.1	0.65	7.1
[45]	SnO_2	ZnO	0.665	16.9	0.58	6.5
[45]	SnO_2	Al_2O_3	0.637	7.0	0.58	2.6
[46]	SnO_2	NiO	0.510	8.6	0.60	2.7
[54]	SnO_2	ZnO	0.590	8.56	0.65	3.28
[47]	SnO_2	ZnO	0.670	11.2	0.69	5.1
[47]	SnO_2	TiO_2	0.660	10.9	0.54	3.9
[47]	SnO_2	ZrO_2	0.550	12.9	0.47	3.4
[47]	SnO_2	MgO	0.600	12.6	0.51	3.8
[47]	SnO_2	Al_2O_3	0.610	9.7	0.61	3.6
[47]	SnO_2	Y_2O_3	0.680	10.7	0.60	4.4
[47]	TiO_2	MgO	0.800	7.0	0.72	4.0
[47]	TiO_2	Al_2O_3	0.740	10.0	0.70	5.2
[47]	TiO_2	Y_2O_3	0.770	6.8	0.75	3.9
[55]	TiO_2	$SrTiO_3$	0.708	10.2	0.58	4.39
[56]	TiO_2	$BaTiO_3$	0.766	16.29	0.61	7.52

CHAPTER 3

EXPERIMENTAL

During this work, in order to construct dye sensitized solar cells from fluorine doped tin dioxide nanoparticles, firstly undoped tin dioxide nanoparticles were synthesized with sol-gel methods. Polymerized complex combustion method and homogeneous precipitation techniques were investigated to obtain nano sized particles with desired morphologies. To dope tin dioxide nanoparticles with fluorine, hydrothermal treatments were conducted inside fluorine containing solutions with different concentrations. For comparison with tin dioxide based cells, titanium dioxide films were also prepared with commercial nanoparticles purchased from Degussa. After preparation of the pastes, screen printing technique was used to deposit nanoparticulate thick films on precleaned transparent and conducting glasses. Surface treatment of the cells were achieved with treating the thick films with titanium precursors like ammonium hexafluoro titanate and titanium tetra chloride aqueous solutions for different dipping durations. Experimental procedures can be categorized under four main steps:

1. Particle synthesis
2. Thick film deposition
3. Surface Modification
4. Dye sensitized solar cell assembly

After successful construction of dye sensitized solar cells, characterizations were made by using simulated AM 1.5 light. Characterizations of the powders and films include X-Ray diffraction, BET surface area measurements, Scanning Electron Microscopy, four point probe resistivity measurements and UV-Visible measurements.

3.1. Particle Synthesis

In order to deposit mesoporous thick films for dye sensitized solar cells, an appropriate particle synthesis technique for obtaining nanopowders with desired morphology and composition is essential. Sol-gel chemistry is a well known, versatile technology to synthesize nanoparticles of various compounds. In this work, sol gel techniques of polymerized complex combustion method and homogeneous precipitation techniques were employed in order to synthesize tin dioxide nanoparticles.

3.1.1. Polymerized Complex Combustion Method

Polymerized complex combustion method (PCCM) or modified Pechini method is different from precipitation techniques which consist of complexing and chelating agents with the material precursor. Resulting mixture is a polymerized complex including metal oxide nanoparticles. In a typical procedure according to a literature report [58], equal amounts of $SnCl_4.5H_2O$ (Aldrich 98%), ethylene glycol (Aldrich 99%) and citric acid (Sigma Aldrich) were dissolved in 100 ml water and ethanol mixture (1:1 vol.) and stirred at 40^oC for 30 minutes for complete dissolution. Resulting mixture was refluxed at 120^oC for 3 hours. After a yellowish solution was obtained, another heat treatment was applied at 80^oC for a day. A brown solid formed and it was further heated at 150^oC until a black-brown powder formed. This powder was heat treated at 500^oC for 2 hours in order to burn organic polymers and complete the crystallizaiton of the powders. A grey powder was formed after heat treatment and powders were characterized with X-Ray diffraction, Scanning Electron Microscopy and BET measurements.

3.1.2. Homogeneous Precipitation Method

Precipitation method is the most convenient method to produce nanoparticles from metal salts which is used widely in ceramic industry. Hydrolysis of metal precursor

occurs upon change of pH of the solution and hydrated particles are obtained from chlorides, alkoxides etc. Tin dioxide nanoparticles were precipitated from $SnCl_4.5H_2O$ using urea (Merck) as the precipitation agent according to literature reports [59, 60]. 0.1 M aqueous $SnCl_4.5H_2O$ solutions were prepared and mixed with ten fold excess urea (1 M). After a completely clear solution was obtained by mixing the solution with a magnetic stirrer for half an hour, solution was refluxed for 10 hours at 90^oC. When temperature of the solution reached 80^oC, urea slowly decomposed to NH_3 and CO_2, increasing the pH of the solution. A turbid occurred after a few minutes and hydrated SnO_2 started to precipitate inside the solution. Complete hydrolysis of $SnCl_4$ to SnO_2 lasted several hours and solution was cooled down to room temperature. Precipitates were removed from the solution by centrifuging and pH of the remaining solution was measured by an electronic pH meter to be around 8-9. The precipitates were further washed with deionized water and centrifuged again. This washing procedure was repeated more than five times to make sure complete removal of Cl^- and NH_4^+ ions. Clean precipitates were dried in drying owen for one day at 100^oC. Dried crystallites were grounded in a mortar and heat treated at 500^oC for 2 hours.

3.1.3. Hydrothermal Treatments

Hydrothermal treatment is a well known technique used to synthesize organic, inorganic compounds and organometallic complexes. Hydrothermal heating has many advantages compared to conventional heating methods combining high temperatures with extreme pressures and allows many compounds to be synthesized in solvents having low boiling points. For hydrothermal treatments applied, a laboratory made stainless steel (316) pressure vessel was constructed to form the autoclave. Inside the vessel, the liner was made up of teflon and all connections and encapsulations were coated with teflon. To measure temperature and pressure inside the vessel, a thermowell and a port connected to a manometer were placed on the top and the autoclave was sealed using stainless steel clamps. Hydrothermal treatments were conducted by heating the autoclave on a hot plate and a magnetic stirrer. Using

this configuration a heating rate of 2^{o}C/min could be achieved and the autoclave cooled down by keeping in air at laboratory conditions.

Figure 3.1 Laboratory made stainless steel autoclave used in hydrothermal treatments.

In this work, hydrothermal treatments were carried out to dope homogeneously precipitated tin dioxide nanoparticles with fluorine. Hydrated particles obtained from precipitation and cleaned by washing, were redispersed in deionized water to form a colloid and inserted into the 270 ml teflon vessel which was placed into the auclave as shown in Figure 3.1. For a safe operation, volume of the solution did not exceed 135 ml. Fluorine doping has been achieved by adding NH_4F (Merck) into the colloid solution. The effect of fluorine concentration on the characteristics of the doped nanoparticles was observed by altering the F/Sn atomic ratio for each treatment. F/Sn ratios of 1, 5, 10, 20, 30, 50 and 100 were tried. After treatment, particles were re-collected by centrifugation and washed with deionized water again. Heat treatments were conducted at 500^{o}C for 2 hours in order to complete crystallization and morphological properties of the powders were characterized by BET, SEM and X-Ray diffraction techniques.

For electrical characterization of the powders, standart four point probe technique has been used. For this purpose, powders were pressed into pellets using a hydrolic pelletizer using around 0.3-0.4 g powder each time. Pellets had a diameter of 5 mm and a thickness of 1 mm.

3.2. Thick Film Deposition

Thick films of tin dioxide, fluorine doped tin dioxide and commercial titanium dioxide nanopowders were deposited on transparent and conducting oxide coated glasses by using screen printing technique. Choice of TCO glasses used in this work were fluorine doped tin dioxide purchased from Solaronix SA (Switzerland) having a sheet resistance of 7 ohm/sq and visible light transmission of around 80% according to the supplier's website. Deposition of thick films includes five steps:

- Preparation of screen printing pastes
- Cleaning of the TCO glasses
- Screen Printing
- Heat Treatment
- Characterization

3.2.1. Preparation of Screen Printing Pastes

Deposition of synthesized nanopowders was achieved by screen printing the pastes including the powders of desired nanoparticles. A screen printing paste is an organic vehicle consisting of high viscosity fluid, the binder to hold particles together before sintering and the target powders. In this work metal oxide nanoparticles were dispersed in terpineol (anhydrous, Fluka) as the carrier and ethyl cellulose (Aldrich) as the binder. For this purpose synthesized nanopowders were first grinded in a mortar and ethanol was added slowly to the mortar. In order to avoid formation of large aggregates, ethanol was added drop by drop under constant grinding. After adding an amount of 30 ml ethanol, the homogeneous colloid was transferred to a beaker using excess ethanol and completed to approximately 100 ml. This colloid

was sonicated for 10 minutes using an ultrasonic titanium horn. The sonication was followed by stirring the colloid by a magnetic stirrer and repeating the sonication again. After dispersion of the particles, terpineol was added to this solution under stirring and the sonication was repeated. A solution of ethanol and ethyl cellulose (10% wt.) was prepared meanwhile by stirring the solution for about half an hour. This solution was added to the terpineol-ethanol mixture under stirring and final solution was sonicated for 15 minutes and mixed for 1 minute. The composition of final solution is 20% metal oxide powder, 10% ethyl cellulose and 70% terpineol and excess ethanol. This excess ethanol was evaporated in a laboratory rotary evaporator at 40^{o}C and spinning for about 6-7 hours until evaporation of ethanol stopped. Resulting mixture is a highly viscous paste containing the desired metal oxide nanopowders. This paste was sealed with a parafilm to avoid evaporation of terpineol and kept for months until the end of work.

3.2.2. Substrate Cleaning

Fluorine doped tin dioxide coated glasses were used as substrates. For good adhesion of thick films on the substrates, clean and inclusion free surfaces are essential. In order to remove organic contaminants and dust, glasses were firstly cleaned in a detergent solution in ultrasonic bath for several minutes. After detergent cleaning, substrates were again cleaned using plenty of deionized water by ultrasonic treatment. Residual organic contaminants were further removed by cleaning the substrates in acetone inside ultrasonic bath for 20 minutes and deionized water again. Cleaned substrates were finally treated with anhydrous ethanol in ultrasonic bath for 20 minutes and kept in ethanol solution until the deposition of thick films.

3.2.3. Screen Printing of Pastes

Screen printing is a well known technique since hundreds of years also referred as silk screen or serigraphy. It is a widely used technique today to deposit thick films on several substrates especially in thick film sensors or micro-circuits. It is a very cheap

and reproducible technique to manufacture any thick films. Infinite types of patterns can easily be formed on the screens by photoemulsions which are made up of fabrics of synthetic or metallic wires attached to wooden or aluminium frames. Screen printing pastes of required fluidity and viscosity are applied on the frames and pastes were squeegeed through the openings of the fabrics where they are applied on the surface. Amount of paste deposited on the surface depends on the thickness of the fabrics while final thickness of the film mostly depends on the concentration of the powders. Figure 3.2 shows stages of screen printing deposition.

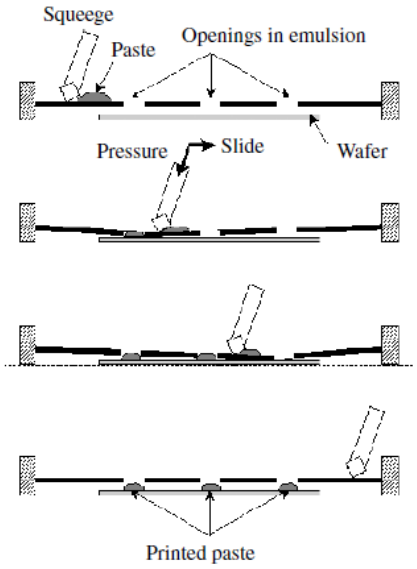

Figure 3.2 Stages of screen printing deposition process [8].

In this work, a polyester mesh stretched in a wooden frame was used as the screen. 10x10 mm and 5x5 mm square patterns were formed by photoemulsion on the screen and used as the template for film deposition, as shown in Figure 3.3. Prepared pastes were applied on 10x10 mm square pre-cleaned glasses on this frame by a rubber squeegee (ragle) for more than one time until the desired thicknesses were achieved referring to the thickness measurements from SEM. The deposited pastes were dried at 120^{o}C for 15 minutes in a drying oven after each paste deposition to remove volatile components of the pastes before each coating repetition and final heat treatment. Before drying the pastes, wet films were kept in dust free closed box for

the paste to relax and reduce surface irregularities caused by the fabrics. All processes were performed in normal laboratory conditions although a dust free clean room is preferrable.

Figure 3.3 Wooden screen used during screen printing deposition.

3.2.4. Heat Treatment of Films

Screen printed pastes of nanopowders have to be heat treated to burn organic compounds in the paste and to complete required sintering of the particles. Sintering time and temperature have to be well chosen to prevent over sintering which results in reduction of porosity and particle growth. When working with soda lime glass, the highest temperature is limited by the softening point of soda lime glass which is around 600^{o}C, over this temperature glass starts to soften and partially melt. Most appropriate temperature for sintering is about 500^{o}C for both titanium dioxide and tin dioxide. Another important issue is the heating rate of the films where sudden changes in temperature result in thermal stresses due to cracking of the film and peeling off from the substrate. As long as the films contain organic binders, these binders have to burn completely before the sintering of particles starts, otherwise organic residues are trapped between interconnected particles and causes failure during the function of the cell. For this reason, a heating regime has been set for the heat treatment. In a typical program, films were first heeated to 325^{o}C with a heating

rate of 10^{o}C per minute and kept at this temperture for 15 minutes. At this stage organic binders and other residues are burned. Another step was 375^{o}C for 15 minutes and finally films were kept at 500^{o}C for half an hour. Hot glasses were kept in the oven and cooled down to room temperature naturally. Unless the films were characterized they were not kept in laboratory medium for long time to prevent contamination from medium.

3.2.5. Characterization

Films were characterized by FEI Quanta 400 FEG field emission scanning electron microscope in Central Laboratory, METU and UV-Visible to determine morphological and optical properties. Prepared films were both observed from surface and cross sections for thickness measurements from cracked and vertically placed films into SEM chamber. UV-Visible measurements were conducted to measure visible light transmission of the films in visible region from 300 to 800 nm using UV-1900 UV-VIS Spectrometer. Films were heated to 120^{o}C for 15 minutes to remove absorbed water and kept in a dessiccator before measurements. X-Ray diffraction analysis was performed by Rigaku D/MAX 2200/PC diffractometer, Metallugical and Materials Engineering department of METU. BET surface area of nanopowders were determined by gas absoption of powders using a Quantachrome Autosorb-6 surface analyzer in Central Laboratory, METU. Before gas absorption measurements, powders were prehetaed at 120^{o}C for 2 hours in order to remove absorbed water. Electrical resistivity measurement of powders were conducted by a Jandel universal four point probe equipped with a Keithley 182 digital voltmeter and Ketihley 238 high current source, in Surface Science Research Laboratory of Metallurgical and Materials Engineering Department of METU.

3.3. Surface Modification with TiO_2

Construction of a core shell type matrix requires modification of the prepared nanocrystalline films with titanium dioxide which results in a tin dioxide core matrix

and a titanium dioxide shell coating. Fresh films of fluorine doped tin dioxide were immersed in aqueous titanium salts and hydrolized TiO_2 precipitated on the sintered and connected particles. Two titanium precursors were used in this work, titanium tetra chloride and ammonium hexafluorotitanate.

For titanium tetra chloride treatments a stock solution of 2M $TiCl_4$ aqueous solution was prepared before treatments. 40 ml $TiCl_4$ was slowly poured into 200 ml deionized water inside an ice bath to prevent rise in temperature because of highly exothermic reaction. This solution was kept in a refrigerator until end of work. Using the stock solution, 40 mmol $TiCl_4$ solutions were prepared and films were immersed into this solution vertically at 70^oC inside a drying oven. Duration of 45 minutes were applied to films and after treatment films were cleaned with plenty of water. A post heat treatment was applied to modified films at 500^oC for half an hour to crystallize the amorphous TiO_2 and adhere to tin dioxide particles. No heating regimes were required at this step.

Ammonium hexafluorotitanate (Aldrich, 99.99%) was hydrolyzed in aqueous boric acid (Sigma-Aldrich 99.5%) solutions and TiO_2 was precipitated onto the films. 0.1 M ammonium hexafluorotitanate and 0.2 M boric acid containing solution was prepared by mixing these two compounds and films were dipped into this solution at room temperature. Durations of 5 minutes, 20 minutes and 45 minutes were applied to the films. After washing with deionized water, films were heat treated again at 500^oC for half an hour.

3.4. Assembly of DSSC

Dye sensitized solar cells were constructed from thick films prepared in the previous section. Cells were assembled in a sandwich configuration according to many literature reports. Five kinds of films were prepared and employed as photoanodes or the working electrode in this work, bare tin dioxide, bare fluorine doped tin dioxide, titanium tetra chloride treated fluorine doped tin dioxide, ammonium

hexafluorotitanate treated fluorine doped tin dioxide and for comparison commercial TiO_2 powders. Remaining components of the cells were purchased fom Solaronix SA and used without further modification. Purchased materials are listed as:

- Fluorine doped tin dioxide coated sodalime glasses, 7 ohm/sq, 80% transmission at 550 nm, 2.2 mm thickness
- Redox electrolyte including 50 mM of triiodide in acetonitrile as solvent with additives ionic liquid, ionic salt and prydine derivatives, model AN-50
- N719 dye as sensitizer (535 bis TBA)
- Platisol platinium precursor
- Surlyn hot melt polymer, 25 micron thickness, model 1170-25

As the performance of the cells strongly depend on cell preparation conditions, care has been taken to prepare every set of identical cells used in this work in the same batch and same conditions for a proper comparison of the examined electrodes.

3.4.1. Dye Staining

Previously prepared working electrodes were stained in dye solution for coloration of films. Commercially purchased N719 dye was dissolved in anhydrous acetonitrile with a molarity of 50 mM and sealed with parafilm to prevent water penetration into dye solution. Films were directly dipped into this solution horizontally and completely wetted by dye solution. This process lasted at least for one day or two days for a proper dye uptake from the solution. Water inclusion from ambient air is a critical parameter affecting the dye molecules absorbed on TiO_2 so films were slowly dipped into the solution while they were around 100^oC after last heat treatment process. After staining the films inside the solution, they were washed by excess acetonitrile or absolute ethanol to remove unbound dye molecules from films. Long storage of the stained electrodes is very detrimental to dye molecules absorbed on the films so after films were cleaned, they were immediately used to construct the cells.

3.4.2. Preparation of Counter Electrode

Counter electrodes containing a thin layer of platinium have been prepared by the platinium precursor containing solution applied on the fluorine doped tin dioxide coated substrate. In order to introduce electrolyte after cell was sealed, a 1mm diameter hole was drilled on the FTO glasses by sandblasting before platinium coating. The cleaning procedure is the same as applied for thick film deposited glass substrates. A drop of platinium precursor solution was dropped on 10x10 mm pre-cutted and cleaned glass substrates and it was spreaded all over the entire surface with a glass rod. After drying the solution in drying oven, films were heat treated at 450^{o}C for 15 minutes. Resulting structure is a thin layer of platinium nano clusters deposited on the glass. As the catalytic activity of platinium is very sensitive to dust and other contaminants coming from the laboratory medium, films were not stored, they were immediately used after heat treatment.

3.4.3. Assembly and Characterization

The working electrode and the counter electrode were brought together to form a sandwich structure by laminating the two glass substrates using hot melt polymer. Cells used in this work have working area of 7x5 mm^2, mostly however these values may alter by 1 mm from cell to cell, giving active areas of 0.35-0.40 cm^2. Surlyn films were cut into frames of the same size with working electrode active areas. The width of the edges of the frames was 1 mm. After placing the frames on the working electrodes carefully, the counter electrode was placed on the working electrode and two glasses were pressed tightly until they stuck each other a little. Hot lamination of the glasses was performed on a previously heated hot plate at around 120^{o}C. After a few seconds, the hot melt polymer started to soften and melt between the two glasses and they were pressed tightly by hand on the hot plate. After 2 minutes cells were removed from the hot plate and cooled down to room temperature. They were examined by eye to make sure no openings or unbound parts are present between two glasses.

Redox electrolyte was introduced into the cells from the predrilled hole on the counter electrode. Under normal conditions the gap between glasses is not fully wetted by the electrolyte placed in the hole so vacuum filling was used. A drop electrolyte was placed on top of the hole and cell was placed into a small vacuum chamber. When the chamber was taken into vacuum, air bubbles started to form inside drop and when the bubbling stopped, chamber was taken into normal conditions where air pressure drived the electrolyte into the gap between the glasses. Excess electrolyte was cleaned from the hole using acetone carefully. The hole was then sealed with Surlyn again by placing a small piece of Surlyn and a cover glass on the hole applying heat by a soldering iron. Silver contacts were applied on the bare edges of the films using a silver paste dissolved in isobuthylmethylketon. Resulting structure is shown in Figure 3.4.

I-V characteristics of the cells were recorded by using AM 1.5 simulated light from an Oriel 96000 Full Spectrum solar simulator employing xenon lamp as light source in Metallurgical and Materials Engineering Department of ITU and Physics Department of METU. Illumination power was calibrated to 100 mW/cm^2. No masks were applied to the cells.

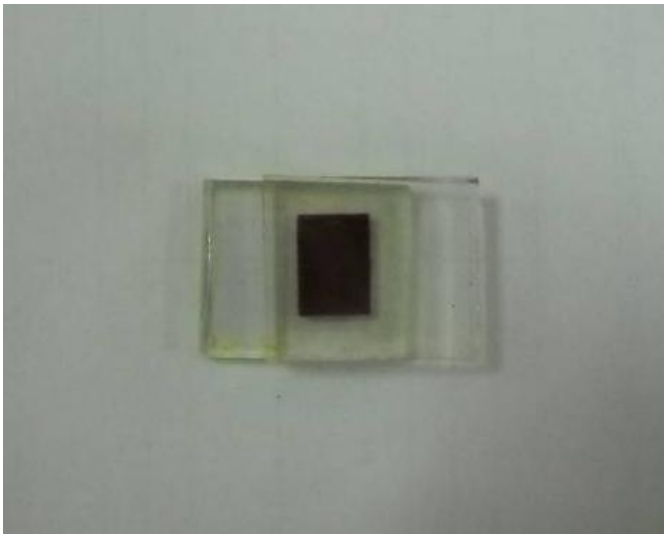

Figure 3.4 A typical dye sensitized solar cell.

CHAPTER 4

RESULTS AND DISCUSSION

In this work, studies have been conducted to construct dye sensitized solar cells employing fluorine doped tin dioxide nanoparticles as core material coated with a thin titanium dioxide layer as the shell material and characterizations were made in order to examine structural properties of the powders and thin films and their effect on the performance of the cells. Obtained particles were characterized with XRD, SEM and BET measurements to identify structural properties like particle size, surface area and crystal structures. Fluorine doped tin dioxide particles were electrically characterized using four point probe method. Optical studies include determination of visible light transmission of deposited thick films by a UV-Visible spectrophotometer. Morphological properties of the films were examined by SEM studies including the thickness measurements of the films. Core-shell type anodes employed as photoanodes of dye sensitized solar cells and characterized by a solar Simulator using AM1.5 simulated light and I-V curves were obtained to compare surface modifications on the performance of the devices.

Structural and compositional properties of the synthesized powders are the most critical parameters for efficient dye sensitized solar cell so it is essential to determine crystal structure and composition of the powders synthesized with homogeneous precipitation and polymerized complex methods. XRD method was used to identify the composition and crystal structure of the powders. XRD data was also used to estimate the particle size of the powders in addition to both SEM and BET analysis. Besides undoped particles, hydrothermally treated particles were also characterized using same tools.

4.1. X-Ray Analysis of Powders

XRD analysis were performed on as synthesized tin dioxide and fluorine doped tin dioxide nanoparticles for determination of crystal structures and compositions of the particles. X-Ray spectra of the particles were recorded for angles between 20-70^{o} for tin dioxide. As the sytnthesized powders have the nanocrystalline nature, mean particle sizes were estimated from Debye- Scherrer equation using the line broadening of the peaks for particle size analysis. Debye-Scherrer formula is given by:

$$t = \frac{\mathrm{K}.\lambda}{B.\cos(\theta)}$$

Eq. [4.1]

In this equation, t is the mean crystallite size, K is the shape factor having the value of 0.94, λ is the wavelength of incoming light where Cu K_{λ} is 1.5418 Å, B is the full width at half maximum in radians and 2θ is the diffraction angle of the peak. Figure 4.1 shows XRD spectra of the tin dioxide powders synthesized from polymerized complex combustion method after sintering at 500^{o}C for 2 hours.

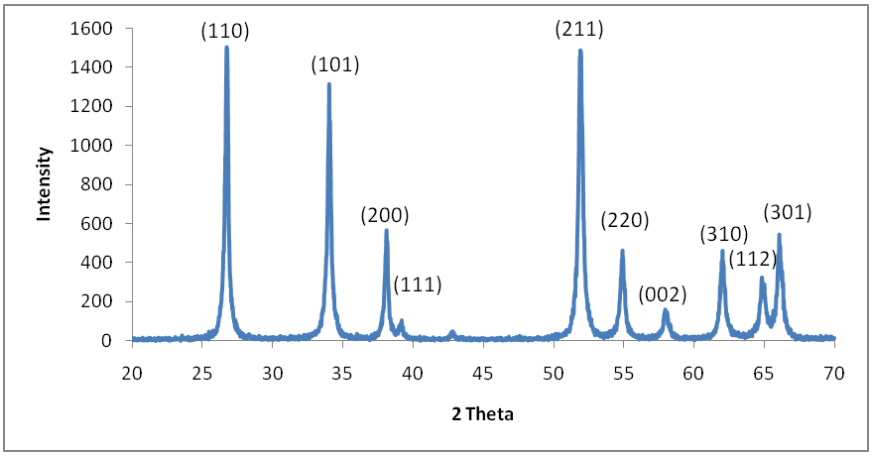

Figure 4.1 X-Ray spectra of tin dioxide powders heat treated at 500^{o}C, obtained by PCCM.

The crystal structure is rutile type cassiterite of tin dioxide (JCPDS 41-1445) without any observed peak for any other elements. High intensity of the spectra indicates that the crsytallinity of the powders are quite good. Mean particle size calculated from broadening of the most intense peak corresponding to (110) plane is 38 nm.

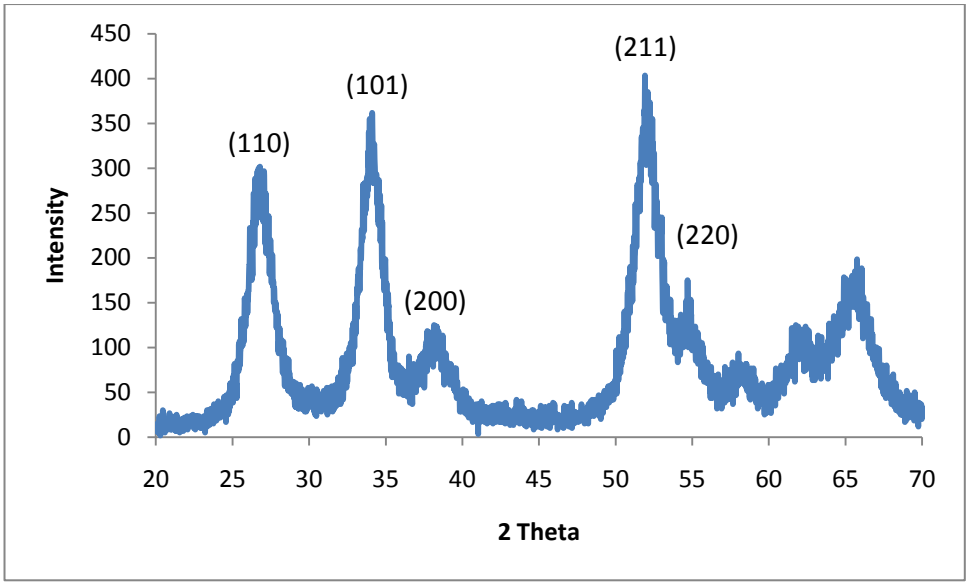

Figure 4.2 As synthesized homogeneously precipitated tin dioxide nanopowders.

Figure 4.2 shows the XRD spectra of as synthesized powders of homogeneously precipitated tin dioxide nanoparticles without any post heat treatment. Structure has very poor crystallinity corresponding to cassiterite type tin dioxide. Particle size estimated from Scherrer equation using the most intense peak of (211) plane is 6.2 nm. Figure 4.3 shows the spectra of the same particles after heat treatment at 500^{o}C for 2 hours.

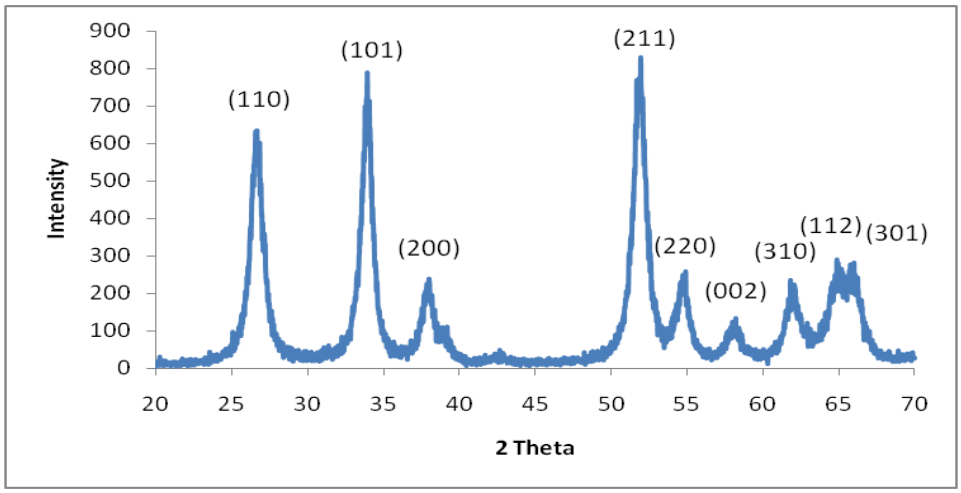

Figure 4.3 X-ray spectra of homogeneously precipitated tin dioxide powders after heat treatment at 500^{o}C.

After heat treatment crystallinity of the particles increases extensively. Mean particle size is around 12 nm indicating a grain and particle growth during the sintering process. Figure 4.4 shows the XRD spectra of tin dioxide nanoparticles after hydrothermal treatment in fluorine contaning solution with F/Sn ratio of 1 and sintered at 500^{o}C for 2 hours.

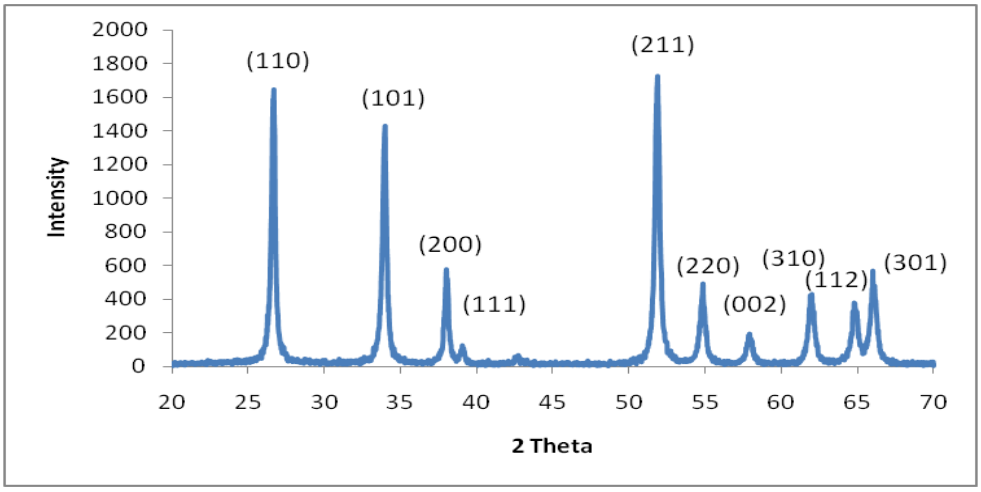

Figure 4.4 X-Ray spectra of fluorine doped tin dioxide nanoparticles after hydrothermal treatment and heat treatment at 500^{o}C for 2 hours.

Structure is cassiterite type tin dioxide with no associated fluorine peak. It seems that fluorine corporation is not sufficient enough during hydrothermal process. Mean particle size estimated from the Scherrer equation using the most intense peak of (211) plane is 15 nm indicating a slight particle growth which must have resulted from the hydrothermal growth of the particles inside the autoclave solution. However, actual particle size has to be determined from BET and SEM analysis of particles for a more proper result as degree of agglomeration cannot be estimated from X-Ray analysis.

4.2. BET Surface Area Analysis of Powders

Nanoparticles used in dye sensitized solar cells are expected to provide high surface areas compared to their bulk counterparts. As the dye molecule absorption on metal oxide occurs on the particle interface, high surface area powders can carry more sensitizer and improved light absorption can be achieved.

Particle sizes calculated from X-Ray analysis give the mean crystallite size contain no information on the surface area of the powders. The agglomeration of the particles during synthesis is common problem and decreases the active surface area of the powders from their theoretical values estimated from particle size. In order to overcome this situation BET (Brunauer-Emmet-Teller) gas absorption measurements were conducted for determining the specific surface area of the powders.

BET surface areas of the powders synthesized in this work have been given in Table 4.1 in comparison with commercial TiO_2 powders.

Table 4.1 Surface areas of synthesized powders and commercial powders.

Powder	Method	Heat Treatment	Surface Area
SnO_2	PCCM	500°C	20.2 m^2/g
SnO_2	Homogeneous Precipitation	As synthesized	155 m^2/g
SnO_2	Homogeneous Precipitation	500°C	54.1 m^2/g
SnO_2 :F	Hydrothermal Treatment	As synthesized	159 m^2/g
SnO_2 :F	Hydrothermal Treatment	500°C	50.1 m^2/g
TiO_2 (P25)		As received	55 m^2/g

Powders of tin dioxide without heat treatment show high surface areas indicating ultra fine particles. Upon heat treatment due to sintering and particle growth, active surface areas of the powders decrease drastically. Application of hydrothermal treatment on homogeneously precipitated particles seems to have little effect on the surface area of these powders. Surface areas around 50 m^2/g are quite suitable for dye sensitized solar cell applications as used in several works. However polymerized complex combustion method used in this work gives insufficient surface areas. This situation may be attributed to high degree of agglomeration in polymerized complex method.

Particle sizes calculated from X-Ray measurements give the average crystallite size rather than active particle size and dispersion. BET analysis can be used to calculate the actual particle size of the powders. Assuming spherical particles, mean particle size of the powders (D) can be related to surface area using the formula [61]:

$$D = \frac{6000}{S_{sp}.\rho_a}$$

Eq. [4.2]

Here, S_{sp} is the specific surface area of powders in m^2/g and ρ_a is the true density of the powders in g/cm^3, 6.95 g/cm^3 for tin dioxide used during calculations. Using this

formula, particle sizes of the powders were calculated and compared to the values obtained from X-ray data as shown in Table 4.2.

Table 4.2 Comparison of particle sizes estimated from XRD and BET measurements.

Powder	Method	Heat Treatment	Particle Size X-ray	Particle Size BET
SnO_2	PCCM	500^oC	38 nm	43 nm
SnO_2	Homogeneous Precipitation	As synthesized	6.2 nm	5.57 nm
SnO_2	Homogeneous Precipitation	500^oC	12 nm	16 nm
SnO_2 :F	Hydrothermal Treatment	500^oC	15 nm	17 nm

The difference between the particle sizes calculated from BET and X-Ray methods is a result of the agglomerated nature of the particles, as the agglomeration increases, active surface area decreases and particles tend to behave like united particles which result in growth of the active particle size of the powders.

4.3. SEM Studies of Powders

Powders synthesized from homogeneous precipitation and polymerized complex combustion method were examined using SEM in order to determine particle size and porosity of the powders. EDX analysis was used for compositional analysis. For SEM studies, a drop of acetone suspension containing the powders were spread on carbon coated sample holders and examined.

Powders used in dye sensitized solar cells in the literature have particle sizes around 20 nm, which is the optimum size for an efficient electronic transport and proper dye

uptake on the surface. It is desirable to achieve a good dispersion of particles which are agglomerate free and individual down to primary particle size. Another important parameter is the size distribution of particles. So far, efforts have been spent to obtain the best distribution of particles. Composition of the powders is important while impurities coming from environment or synthesis conditions is a major factor determining the performance of the cells.

Figure 4.5 and Figure 4.6 show tin dioxide powders synthesized with polymerized complex combustion method, sintered at 500^{o}C for 2 hours.

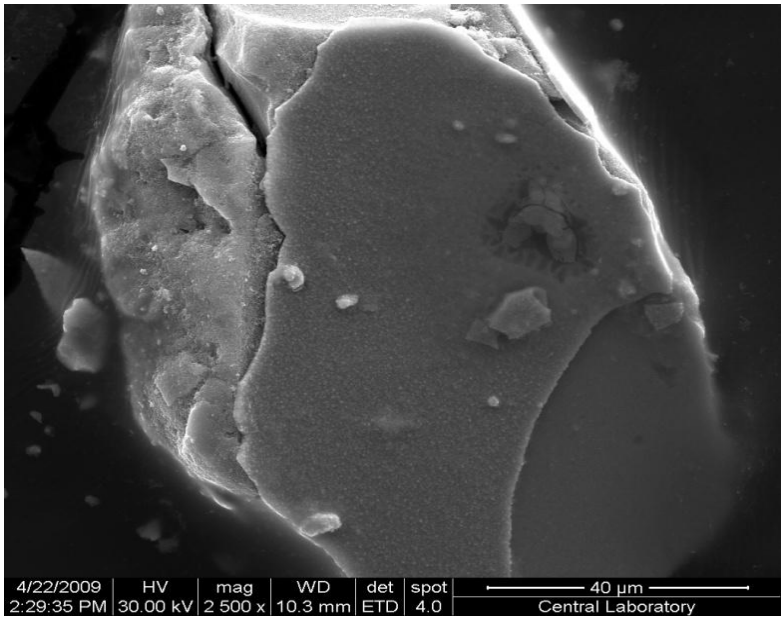

Figure 4.5 SEM image of a large tin dioxide agglomerate synthesized with PCCM and sintered at 500^{o}C for 2 hours.

Figure 4.6 shows the surface of the large agglomerate shown in Figure 4.5. It can be seen that this agglomerate of 60 micron contains very small particles sintered together to form a bigger agglomerate.

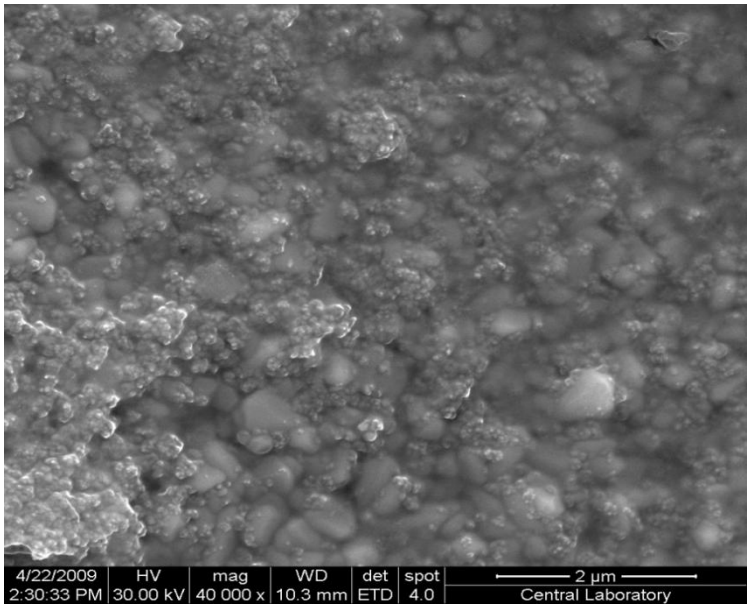

Figure 4.6 Magnified SEM image of surface of the tin dioxide agglomerate shown in Figure 4.5.

The agglomerated nature of powders synthesized from polymerized complex method is obvious from the figures. From Figure 4.6, it is seen that smaller particles of tin dioxide particles are distributed through a network of bigger particles of around 800 nm which are also bound together to form large particles. These results are also in agreement with the BET analysis although XRD results calculated from Scherrer equation gives smaller particle sizes. This difference may be attributed to the fact that large particles are formed by the association of smaller particles which act like individual grains.

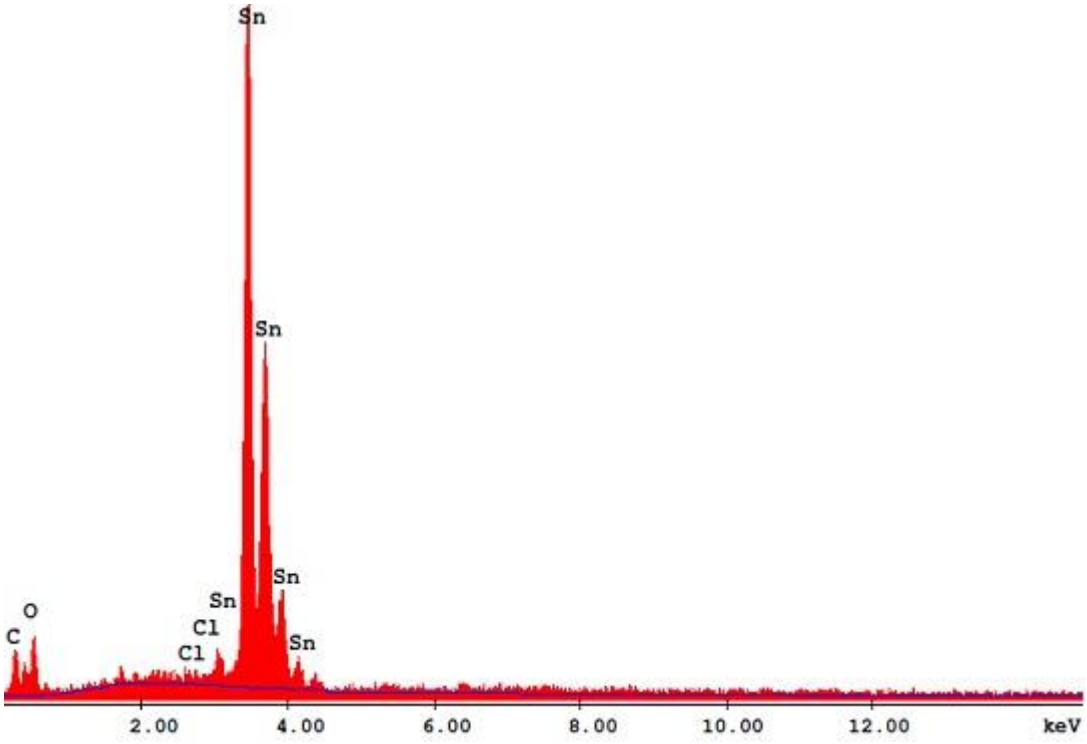

Figure 4.7 EDX spectra of tin dioxide powders synthesized with PCCM.

Figure 4.7 shows the EDX spectra of the powders (34.85% C, 40.79% O, 0.48% Cl, 23.37% Sn atomic ratio). It contains very small amount of chlorine contamination. This excess chlorine is attributed to $SnCl_4.5H_2O$ precursor and remains in the structure as no washing procedure was applied to powders which also cannot be removed by thermal treatment. Presence of carbon is a consequence of the carbon sample holders.

Powders of homogenous precipitation achieving higher surface areas than polymerized complex method are estimated to have lower particle sizes and less agglomeration. Figure 4.8 shows SEM images of homogeneously precipitated powders after drying and without thermal treatment indicating the decrease in the particle size due to homogeneous precipitation.

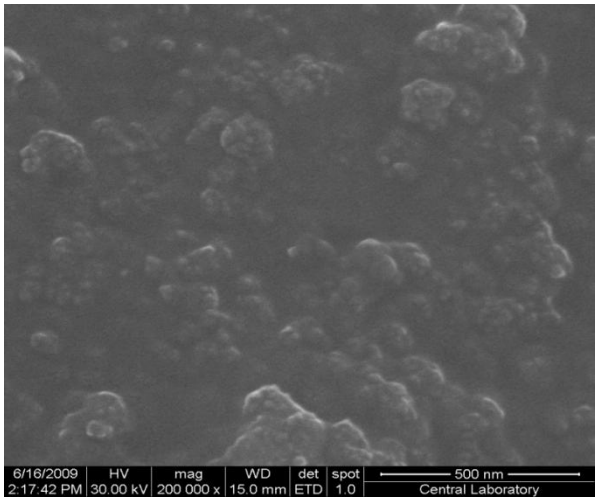

Figure 4.8 SEM image of as synthesized homogeneously precipitated tin dioxide.

According to BET results and XRD analysis these powders have particle sizes around less than 10 nm and it is seen that these ultrafine particles are associated together to form bigger particles. It is not possible to determine the actual size of the particles as a result of poor resolution of the images. Figure 4.9 shows SEM image of the same particles after thermal treatment at 500^{o}C.

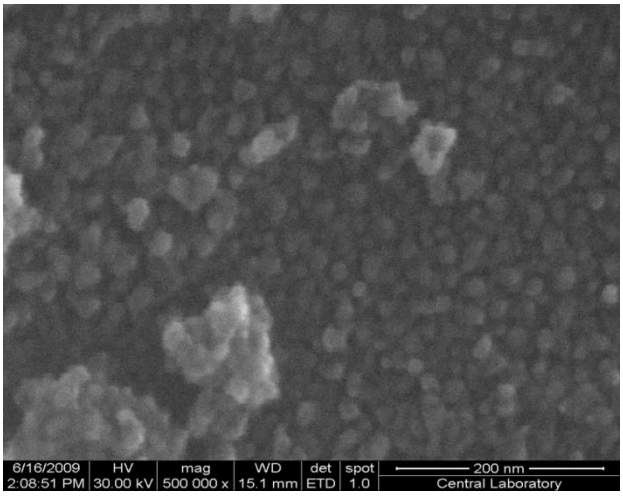

Figure 4.9 SEM image of homogeneously precipitated tin dioxide particles after heat treatment at 500^{o}C.

Heat treatment of the as synthesized powders results in particle growth and crystallization of the particles. As synthesized powders with ultra fine particles have a particle size of around 10-15 nm after heat tretament which can be clearly observed from figure. Although particle size distribution is not very good and agglomeration is not fully prevented, tin dioxide particles of 15 nm diameter have been achieved using homogeneous precipitation method. This value is consistent with the particle sizes obtained from precipitation techniques from literature and fulfill the optimum particle size for dye sensitized solar cells with the surface area value around 50 m^2/g.

EDX spectra of these homogeneously precipitated powders is given in Figure 4.10 (65.93% C, 12.92% O, 20% Sn atomic ratio). There is no peak indicating the presence of chlorine contamination which shows that washing procedure of the precipitates achieves complete removal of impurity ions.

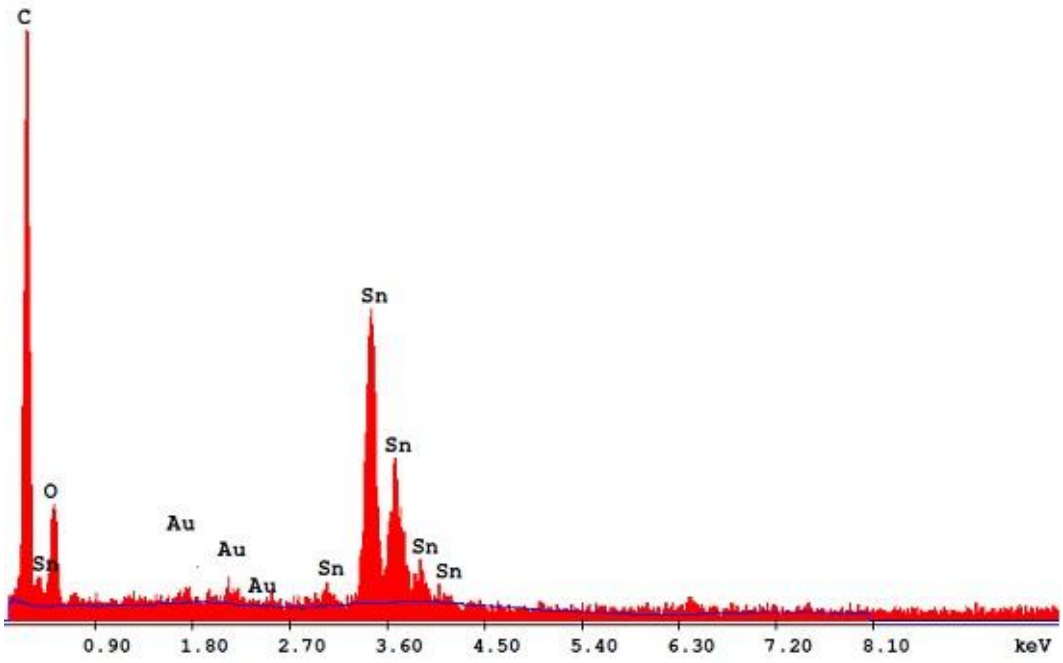

Figure 4.10 EDX spectra of homogeneously precipitated tin dioxide powders.

Precipitates of homogeneous precipitation method were autoclaved using fluorine containing solutions after washing and fluorine doping achieved in aqueous media.

SEM images of powders after hydrothermal treatments in solutions containing fluorine with F/Sn ratio of 1, are given in Figure 4.11 and Figure 4.12 before and after heat treatment at 500^{o}C.

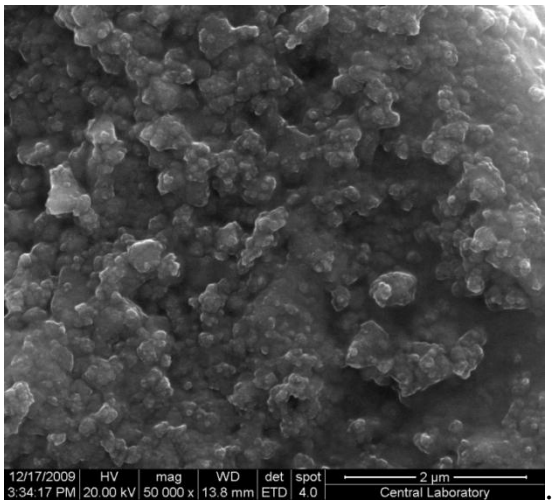

Figure 4.11 SEM image of fluorine doped tin dioxide (FTO) nanopowders after hydrothermal treatment.

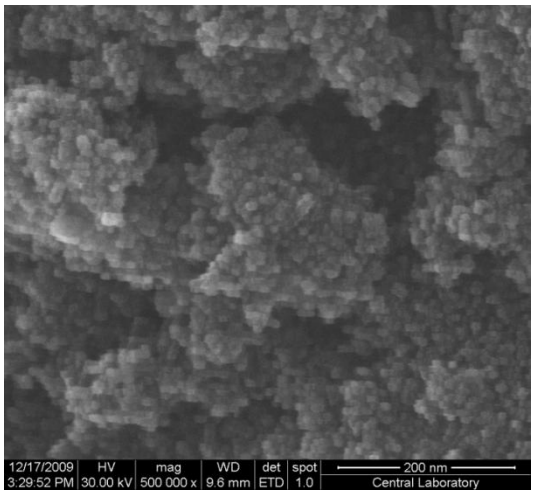

Figure 4.12 SEM image of FTO nanopowders after heat treatment at 500 ^{o}C.

Morphology of the particles after hydrothermal treatments are quite similar to those without treatment. There is no significant change in both surface area and particle

sizes of the particles associated with hydrothermal treatment. Particle sizes are around 10-20 nm which are agglomerated to form larger particles. Figure 4.12 shows a typical structure of the powders where mesoporosity is also observable. Although a particle dispersion down to primary particle size is still not available, this structure is quite suitable for dye sensitized solar cell applications achieving high surface areas and porosity together in contrast to polymerized complex method. Because of this reason, only powders obtained from precipitation method and hydrothermal treatments were used as core materials in the cells so thick films of these powders were deposited and characterized.

4.4. Electrical Characterization of Powders

Effect of fluorine doping using hydrothermal treatment on tin dioxide nanoparticles has been investigated by measuring the electrical resistivity of the powders. For this purpose four point resistivity measurements were conducted on compact pellets of powders and effect of fluorine concentration on the resistivity of the pellets was investigated.

Electrical resistivity ρ of thick samples measured using the four point arrangement is given by the equation:

$$\rho = \mathrm{G}\frac{\mathrm{V}}{\mathrm{I}}$$

Eq. [4.3]

where I is the applied current and V is the measured potential. G is a shape factor depending on the thickness and dimensions of the samples having the form [62]:

$$G = 2\pi \mathrm{s}\mathrm{T}_{\mathrm{g}}\left(\frac{\mathrm{t}}{\mathrm{s}}\right)$$

Eq. [4.4]

In this equation, s is the probe spacing of 1 mm and $T_g(t/s)$ is a shape factor depending on ratio of thickness to the probe spacing and used as 0.6 for the pellets [62].

Figure 4.13 shows the measured values of the resistivities of powders against fluorine content in the autoclave solution.

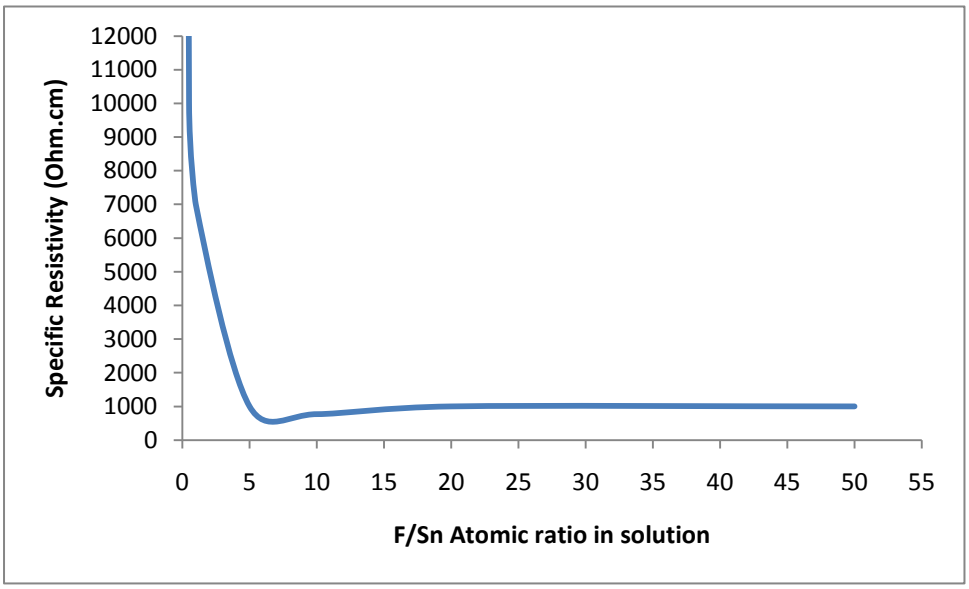

Figure 4.13 Specific resistivity values of FTO particles vs. F/Sn atomic ratio inside the starting solution.

Since tin dioxide is an insulator material in its pure form, resistivities of the powders are on the order of 10 kΩ.cm. Upon fluorine incorporation into the lattice, values decrease some extent, to 770 Ω.cm as the lowest resistivity value obtained in this work. Increasing the fluorine content inside the solution causes no more decrease in the resistivity and this value remains almost unchanged even for 5000 % (F/Sn is 50).

Although there is a decrease in the resistivity of the powders compared to undoped tin dioxide, resistivity is still too high and inferior compared to fluorine doped tin dioxide thin film coatings deposited by CVD, PVD and spray pyrolysis where values

around 10^{-4} Ω.cm can be obtained with these methods. This result shows that fluorine inside the solution is not incorporated into tin dioxide lattice sufficiently while the reason of this increase in conductivity is the substitutional replacement of oxygen in the lattice by fluorine which could not however be detected by X-ray measurements.

4.5. SEM Studies of Thick Films

In dye sensitized solar cells, it is important to deposit films which are well adhered to the substrate and are crack free for an efficient electron transport from mesoporous matrix to the TCO (transparent conducting oxide) current collector. Thickness of the films is an other important parameter directly influencing the overall conversion efficiency. For proper comparison between different anodes used in the cells, determination of thickness and morphology of the films are essential. Although pastes used for depositing the films have the same particle and binder composition, final results have to be observed.

For constructing fluorine doped tin dioxide particle based solar cells, powders obtained by homogeneous precipitation and following hydrothermal treatments were deposited on TCO glasses by screen printing technique. After screen printing of the pastes, all films were heat treated at 500^{o}C for 45 minutes. For comparison between titanium dioxide and tin dioxide nanoparticles employed in the cells, SEM images of both titanium dioxide and fluorine doped tin dioxide film surfaces were taken and in order to determine the thickness of the coating, cross sectional images were recorded. Figure 4.14 shows the surface of P25 (commercial TiO_2 particles) films deposited by screen printing using two coating cycles.

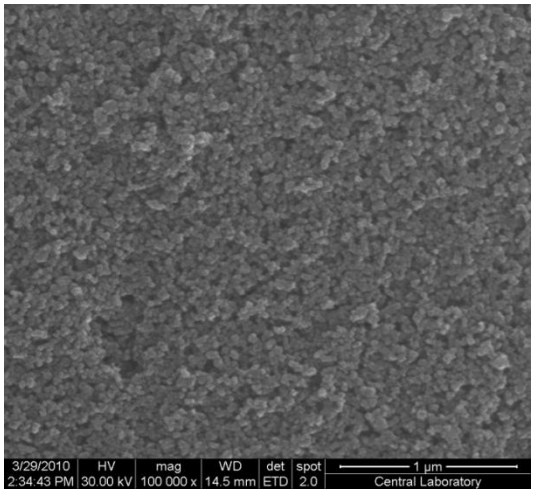

Figure 4.14 SEM image of P25 thick films from top view.

As seen in Figure 4.14, films obtained by using commercial Degussa P25 TiO_2 particles show a fine particle dispersion and there are no observed large agglomerates in the structure. Particle size is around 20-25 nm for these commercial powders consistent with the supplier information. Mesoporosity is also observable which is an important necessity for the production of dye sensitized solar cells.

Figure 4.15 and Figure 4.16 show the cross sectional images of the coatings.

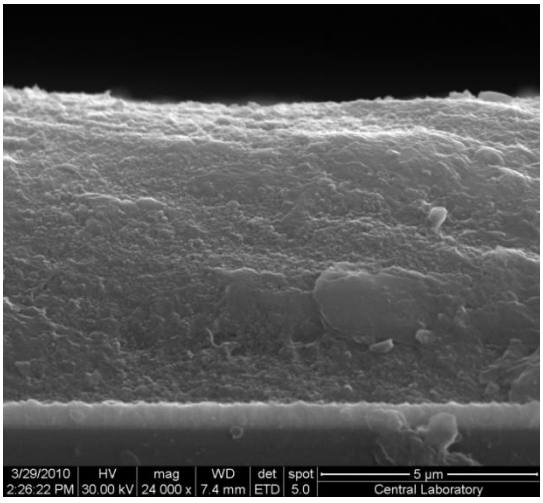

Figure 4.15 Cross sectional SEM image of P25 thick films.

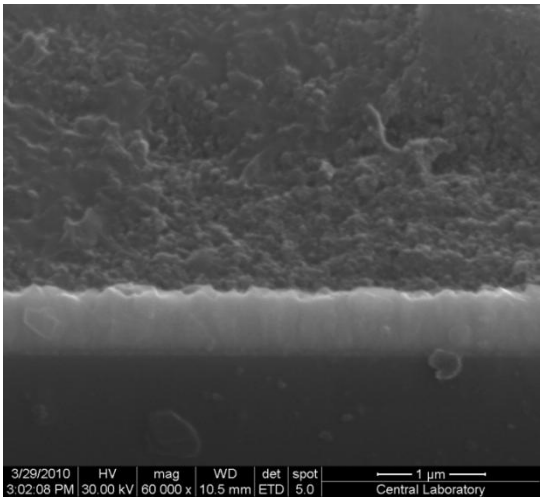

Figure 4.16 Magnified cross sectional SEM image of P25 films.

It can be seen that the films are well adhered to the FTO glass substrate and thicknes is uniform in microscale. Pastes prepared with P25 particles give about 6.5 micron thickness using 2 coating cycles and with each coating giving about 3 micron thickness.

The thickness of the films after 4 printing cycles has been shown in Figure 4.17.

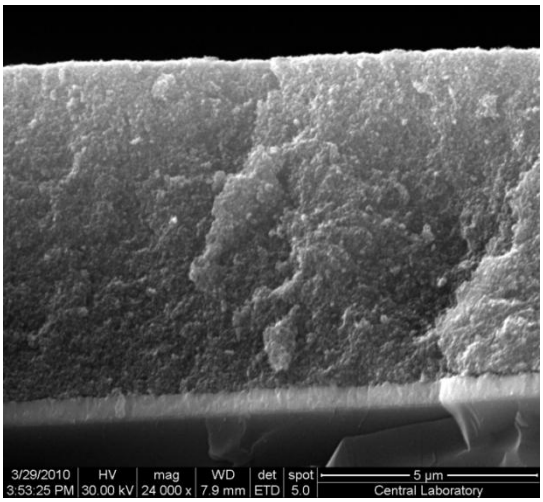

Figure 4.17 Cross sectional SEM image of P25 films for 4 printing cycles.

Films after 4 printing cycles give a thickness of 11 micron which corresponds to approximately 2.5 micron for each coating step. This is a common situation for thick films deposited from screen printing pastes where coating thickness does not increase linearly with coating cycles. It is also seen that increasing the thickness of the films has no effect on the morphology and adherence properties of the films to the substrate as they are well adhered to the glass without any significant coating failure.

Surface morphology of thick films deposited by pastes using fluorine doped tin dioxide nanoparticles synthesized by hydrothermal method are shown in Figure 4.18. Magnified images of the same film are shown in Figure 4.19 and Figure 4.20.

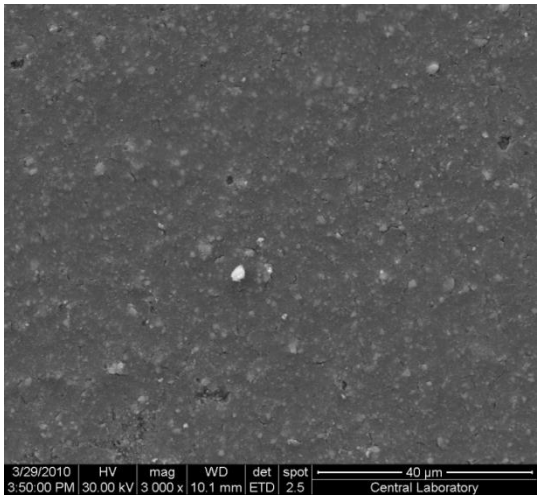

Figure 4.18 SEM image of FTO nanopowder thick films (top view).

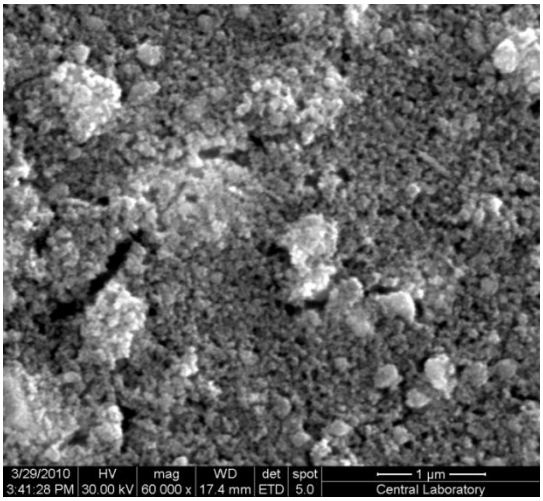

Figure 4.19 Magnified image of the film in Figure 4.18.

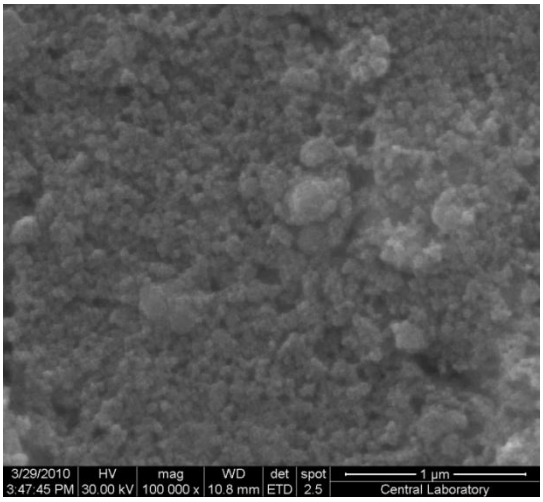

Figure 4.20 Magnified image of the film in Figure 4.18.

In contrast to P25 films, there is agglomeration to some extent in these films. Agglomerates of nanoparticles up to 500 nm are present in the structure and distributed all over the films. Mesoporosity is also observable from magnified images as it is in P25 films.

Cross sectional image of fluorine doped tin dioxide nanoparticle thick films on fluorine doped tin dioxide coated glass substrate is shown in Figure 4.21 for 2 printing cycles. Figure 4.22 shows magnified image of the same film close to the film and FTO coating interface.

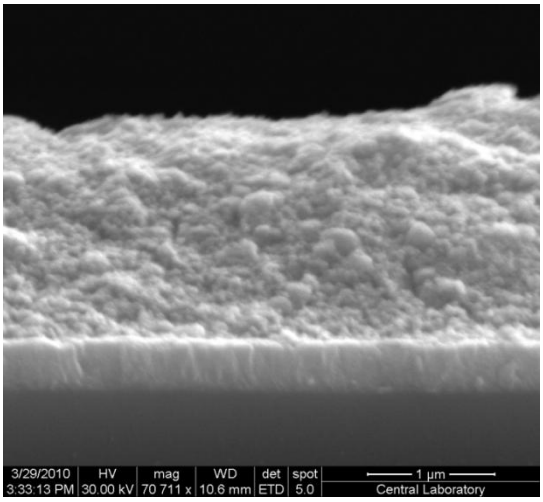

Figure 4.21 Cross sectional SEM image of FTO nanoparticle thick film.

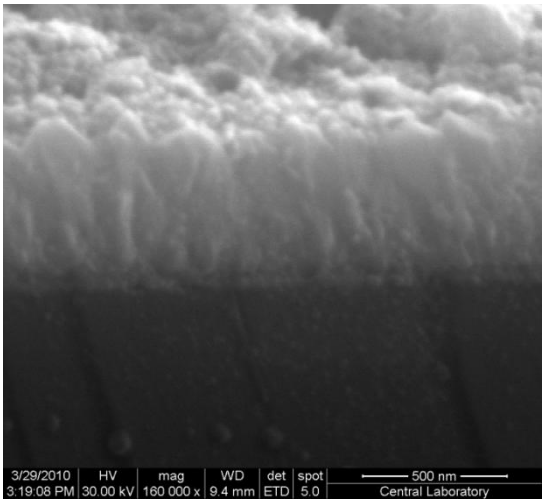

Figure 4.22 Cross sectional magnified SEM image of FTO nanoparticle thick film.

It is seen that films have a thickness of 3 microns for 2 cycles of printing where each printing cycle gives a thickness of 1.5 micron as compared to 2.5 micron cycle thickness for P25 films. Large aggregates can also be seen in these figures. The particles are well adhered to the films without any cracks as this situation can be expected from the fact that both layers are fluorine doped tin dioxide and adhere each other well.

SEM studies of the screen printed films of fluorine doped tin dioxide and commercial titanium dioxide nanoparticles show that films are deposited on FTO glass substrates properly and they are well adhered to the substrates. Mesoporosity has also been achieved and films suitable for dye sensitized solar cell applications were obtained using the FTO nanoparticles synthesized in this work.

P25 films are homogeneous and agglomeration free in contrast to fluorine doped tin dioxide particles. Agglomeration of tin dioxide results from the powder preparation conditions where homogeneous precipitation was used for the synthesis. In the previous section, it was observed that as prepared powders contain large aggregates and it is obvious that these aggregates cannot be broken down after paste preparation and they are present in the structure. However, these large aggregates do not cause failure of the films and do not result in peeling off because it is seen that they are adhered to the films. Although presence of large aggregates in the films of tin dioxide particles does not affect mechanical properties of the films, optical properties of the films may alter beacause of these aggregates which is discussed in the next section.

4.6. Optical Properties of Thick Films

Optical properties of the thick films deposited by screen printing were analyzed with UV-Visible transmission studies. Operation and efficiency of dye sensitized solar cells are highly affected by the light-sensitizer interaction and hence optical properties of anode is quite important for an efficient light absorption.

Wide band gap metal oxides employed in dye sensitized solar cells are normally transparent in the visible light region of the solar spectrum and no absorption occurs in the metal oxide layer. Due to this property, high transparency can be obtained in these cells. However, for high efficiency devices, it is desirable to capture as much light as possible of the solar spectrum.

Figure 4.23 shows UV-Visible spectra of 8 micron thick P25 coating on soda lime glass substrates. Appearance of the coating is transparent and slightly blue. It is seen that absorption edge is around 400 nm at which band to band electronic transitions start and TiO_2 nanoparticles start to absorb ultraviolet light. UV-Visible spectra of the fluorine doped tin dioxide coating prepared by using nanoparticles synthesized in this work is given in Figure 4.24.

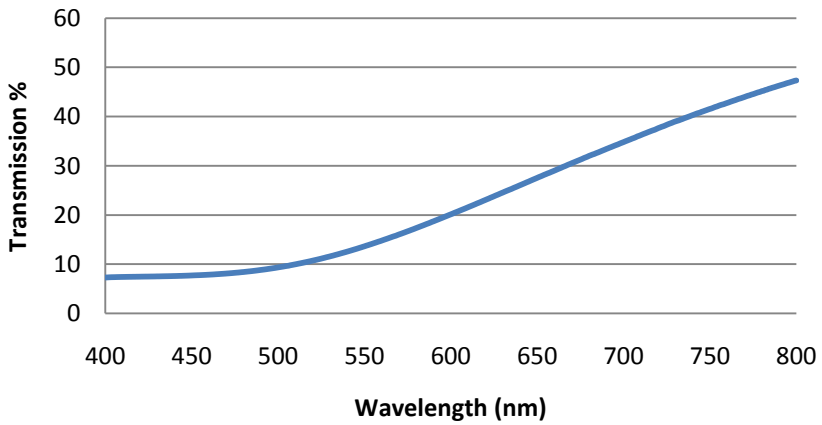

Figure 4.23 UV-Visible specta of P25 thick films.

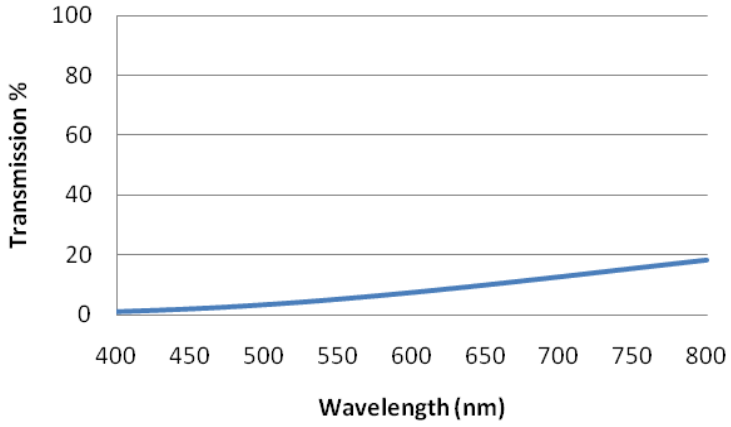

Figure 4.24 UV-Visible spectra of FTO thick films.

Tin dioxide coating has no transparency and is completely opaque and white colored. This can also be seen from the transmission spectrum where most of the visible light is not transmitted through the FTO film. As tin dioxide is also a wide band gap semiconductor as titanium dioxide, it is expected to have the same transparency as the P25 films. The difference in transparency is attributed to large aggregates present in the tin dioxide films. It is known that particles larger than 100 nm can effectively scatter visible light and films made from large particles are mostly opaque. Although particle size of the tin dioxide particles are around 20 nm, large aggregates of particles act like light scattering centers inside the film, so films does not show transparency as P25 films do. However, introduction of haze is usually desirable for the case of dye sensitized solar cells while scattering of visible light by large particles causes light trapping effect inside the cells and improves light harvesting efficiency and cell performance. Effect of this situation on the solar cell parameters is discussed in cell characterization part.

4.7. Characterization of Solar Cells

Dye sensitized solar cells were constructed from fluorine doped tin dioxide thick films after modification with titanium dioxide, which resulted in a tin dioxide core matrix and a titanium dioxide shell coating. Titanium dioxide shell was deposited by

hydrolysis of ammonium hexafluorotitanate and titanium tetrachloride in aqueous solutions, and effect of surface modification on cell parameters were determined by using simulated AM 1.5 light calibrated to give 100 mV/cm^2 and recording the I-V curves of the cells.

Efficiency (η) of a solar cell is simply the ratio of maximum power output of the cell P_{MP} to the power of incident light P_{in} given by [7]:

$$\eta = \frac{P_{MP}}{P_{in}}$$

Eq. [4.5]

Maximum power output of a solar cell is defined by the maximum power point, where product of current and potential has the highest value when a load is connected to the device. In open circuit conditons where there is no current flowing inside the cell, voltage has the maximum value. In short circuit conditions, when there is no potential difference, current is maximum. In real conditions, when there is a resistive load on the circuit, both short circuit current and open circuit voltage values of the cell start to decrease and maximum power output of the cell is defined as the maximum value of product of current and the corresponding potential. This value depends on the ability of solar cell to supply as much power as possible to the load and it is determined by the fill factor of the cell. Fill factor is a useful quantity to characterize solar cells which is mostly influenced by the internal resistances of the cells as well as electron losses inside the cells. It is given by ratio of maximum current I_{MP} and voltage V_{MP} to the short circuit current I_{SC} and open circuit voltage V_{OC} as [7]:

$$FF = \frac{I_{MP}\, V_{MP}}{I_{OC}\, V_{OC}}$$

Eq. [4.6]

As the performance of the cells are highly affected by the preparation conditions and dimensions of the cells, care has been taken to construct cells with similar active areas and as identical as possible to prevent additional resistive elements and influence on fill factors of the devices.

Figure 4.25 shows I-V curve of a dye sensitized solar cell constructed from bare fluorine doped tin dioxide coating of approximately 8 micron thickness without any surface modification.

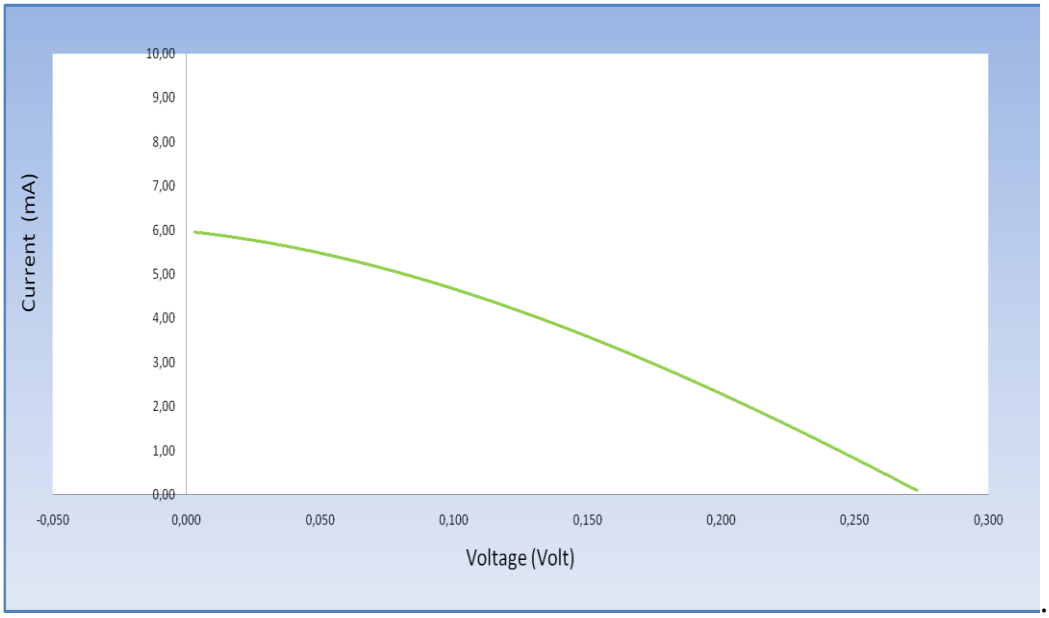

Figure 4.25 I-V characteristics of bare FTO cells.

Efficiency of the cell is 1.165 % with an active area of 0.45 cm^2, showing both inferior open circuit potential and short circuit with a fill factor of 0.32 compared to P25 TiO_2 films shown in Figure 4.26.

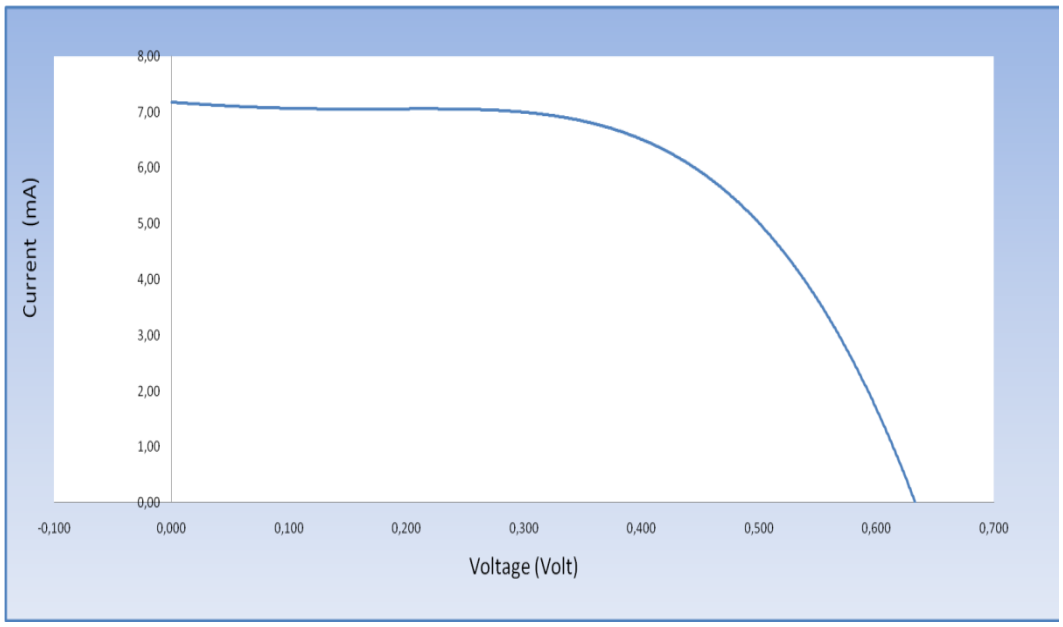

Figure 4.26 I-V characteristic of P25 TiO_2 cells.

TiO_2 cells give efficiency of 6.54 % and shows a fill factor of 0.6 at 0.4 cm^2. Although current densities are comparable between two cells, high fill factor and potential is the main reason of the difference of two cells as expected from literature examples. High recombination rate of cells constructed from tin dioxide decreases both fill factor and maximum voltage resulting in poor efficiencies.

The TiO_2 shell outer layer was deposited from ammonium hexafluorotitanate (AHFT) on fluorine doped tin dioxide for 5, 20 and 45 minutes. I-V curves of these cells are given in Figure 4.27.

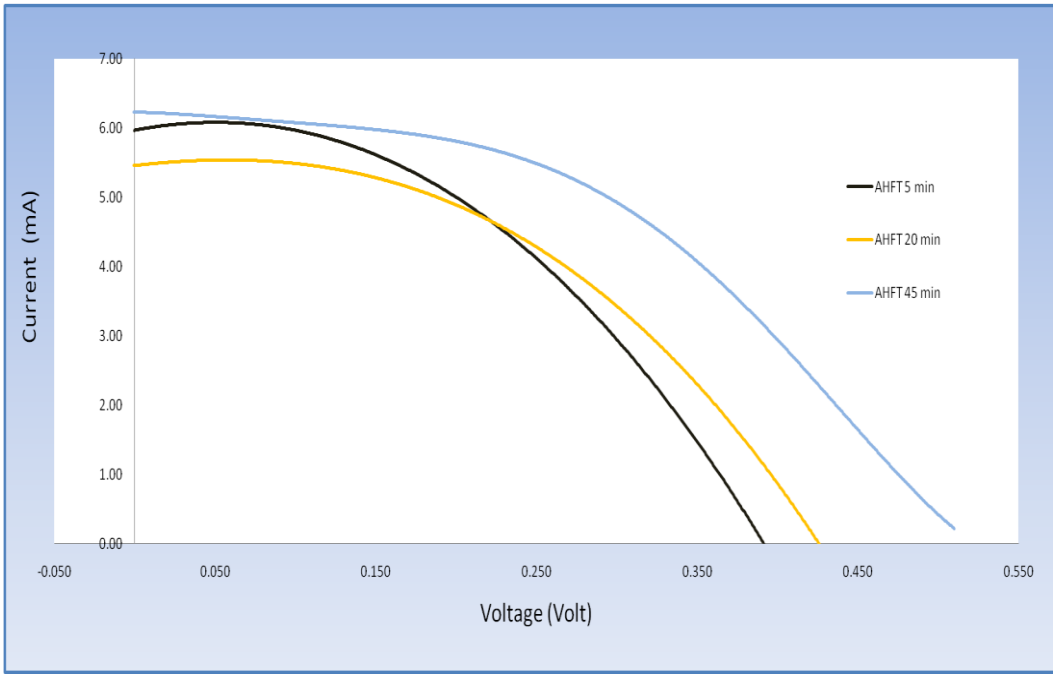

Figure 4.27 I-V characteristics of cells treated with AHFT.

Efficiencies of the cells are 3.1 %, 3.3 %, and 3.79 %, respectively. It is obvious that coating the tin dioxide surface with TiO_2 extensively increases the efficiency of bare tin dioxide cells. Increasing the duration time also enhances the efficiency which is attributed to an increase in the potential where current densities are remained nearly unchanged.

I-V curves of the cells treated with titanium tetrachloride solution is given in Figure 4.28. Efficiency of the device is 4.61 % with enhanced potential and photocurrent simultaneously. Photocurrent enhancement is even higher than that of pure TiO_2 cells, however voltage and fill factor are stil lower.

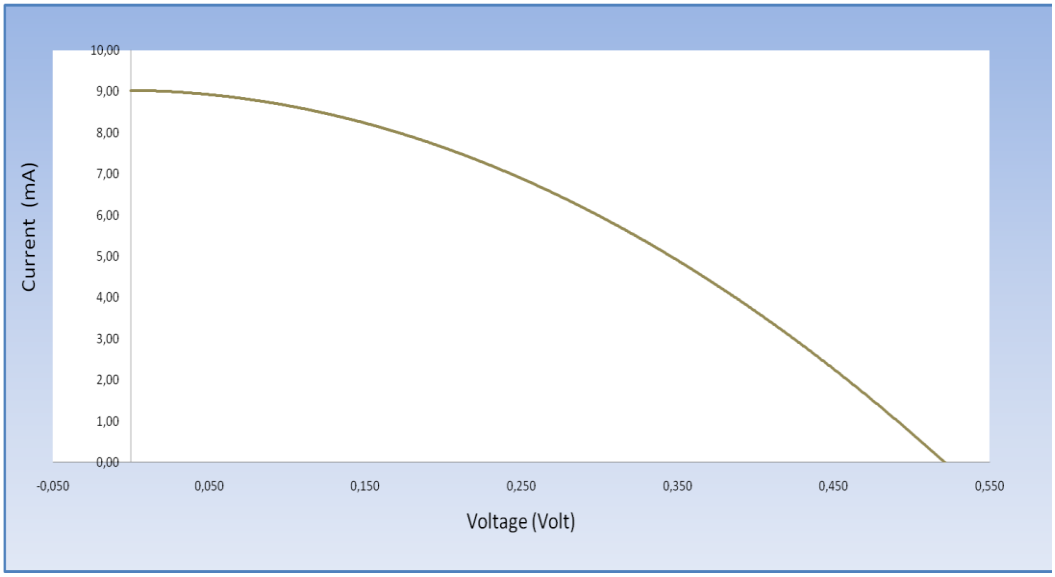

Figure 4.28 I-V characteristics of cells treated with $TiCl_4$.

Table 4.3 summarizes cell parameters obtained in this work. It is obvious that coating the surface of fluorine doped tin dioxide nanoparticles with TiO_2 enhances the overall efficiency of the cells. Increasing the ammoniumhexafluorotitanate treatment duration increases the photovoltage while fill factors remain almost the same.

There is a sharp decrease in the photocurrent of the cells treated for 45 minutes. This situation can be attributed to a decrease in the internal surface area of the structure due to excess TiO_2 deposition into the pores of the matrix and this may result in poor electrolyte diffusion as well as decreased dye absorption resulting from decreased internal surface area. However, increase in the photovoltage which is not directly related to ionic or electronic transport, causes higher efficiency. It is concluded that there is an optimum TiO_2 shell thickness for such core shell type structures.

Table 4.3 Summary of cell parameters of dye sensitized solar cells constructed in this work.

Sample	**Treatment**	**Active Area (cm^2)**	**V_{oc} (V)**	**J_{sc} (mA/cm^2)**	**Fill Factor**	**Efficiency (%)**
Bare SnO_2 :F	-	0.45	0.273	13.2	0.32	*1.165*
TiO_2 P25	-	0.40	0.634	18.75	0.60	*6.54*
SnO_2 :F	AHFT 5 min	0.35	0.395	17.28	0.45	*3.105*
SnO_2 :F	AHFT 20 min	0.33	0.427	17.12	0.45	*3.3*
SnO_2 :F	AHFT 45 min	0.45	0.510	13.91	0.54	*3.79*
SnO_2 :F	$TiCl_4$ 45 min	0.39	0.523	22.82	0.39	*4.61*

Application of titanium tetrachloride treatment gives the best results for core shell type cells in this work. Both photovoltage and photocurrent were enhanced compared to cells treated with AHFT although fill factor is at the same order. This situation can be related to a better coverage of tin dioxide surface as the hydrolysis rate of $TiCl_4$ is slower than AHFT where high hydrolysis rates result in a more particle like deposition of TiO_2 instead of a full coverage of the particle surface. However this situation has to be confirmed by intense TEM work on the morphology of the coatings.

Photocurrents of SnO_2 cells competing with and even higher than TiO_2 cell in this work may be attributed to the difference between optical properties of the coating where there is a high degree of light scattering inside the fluorine doped tin dioxide

films in contrast to TiO_2 films which enhances the light absorption and increase the photocurrent. For a meaningful comparison, it is desirable to introduce same amount of haze into the TiO_2 films by adding larger particles. However, high photocurrent is also expected from SnO_2 cells as higher electron mobility and electronic conduction results in better collection efficiencies.

The main reason of the high efficiency of TiO_2 compared to other metal oxides and SnO_2 arises from the fact that TiO_2 cells shows high fill factors and photovoltages. The origin of the high voltage is that conduction band edge of TiO_2 is close to the LUMO of dye molecule and thus fermi level of injected electrons is higher than SnO_2 which has a conduction band edge at more positive values. This situation causes lower chemical potential between fermi level and redox potential of the iodide/triiodide couple in the electrolyte. Coating the surface of SnO_2 with TiO_2 or other metal oxides shifts the fermi level of electrons and higher potentials can be obtained.

The shell coating acts like a barrier layer between electrons injected to SnO_2 layer and electrolyte which suppresses the recombination of photoelectrons with triiodide. This situation both enhances photocurrent and photovoltage. However, poor fill factor of the cell indicates that recombination is still high at the uncovered parts of the SnO_2 and fill factors still lower than TiO_2. But it is quite promising to obtain such high photocurrents and if recombination can be further suppressed by modifying the surfaces completely, it is believed that higher fill factors, photovoltages and thus efficiencies can be obtained which is a very promising result for future work on this structure.

CHAPTER 5

CONCLUSION AND SUGGESTIONS

During this work, dye sensitized solar cells were succesfully constructed employing fluorine doped tin dioxide as core material and titanium dioxide as the shell material which was proved by XRD, BET, SEM and electrical characterizations.

For the synthesis of tin dioxide nanoparticles, homogeneous precipitation gave better morphological properties like particle size and surface area compared to polymerized complex combustion method. The particles produced in this work with a surface area around 50 m^2/g and particle size of 15 nm are suitable for dye sensitized solar cells and are consistent with the literature. Although there exists some degree of agglomeration in the synthesized powders, these aggregates do not have significant harm on the function of cells, however better size distribution and particle dispersion are always desirable. Hydrothermal treatments showed no change on both morphology of powders and crystal structure of tin dioxide. X-Ray results showed that no fluorine is incorporated into tin dioxide lattice, however electrical characterizations confirmed fluorine substitution with oxygen as there is a small increase in the conductivity of the powders. No further work on the determination of fluorine content inside the particles was conducted in this research and it is suggested to conduct detailed elemental analysis of particles using X-ray Photoelectron Spectroscopy in order to map elemental profile of powders and Hall effect studies can be conducted to determine free carrier concentration which in turn gives information about substitutional fluorine incorporation into the lattice.

Electrical characterization of powders revealed that a decrease in resistivity was achieved, however it is still inferior to conventional thin film deposited FTO

coatings. It was seen that fluorine content inside autoclave solution did not increase the fluorine substitution under conditions of this work. The lowest resistivity value found is 770 ohm.cm for an F/Sn atomic ratio of 5 in the starting solution. This result may be a consequence of low autoclave processing temperature of 180^{o}C and absence of addtional pressure. Application of higher temperatures and increasing the duration of treatment is believed to enhance the desired fluorine doping into tin dioxide particles and lower resistivities can be obtained which in turn will make it possible to deposit films of FTO nanoparticles with sufficient electrical conductivity.

Thick films of fluorine doped tin dioxide and commercial TiO_2 powders were deposited on TCO glass substrates by screen printing technique successfully. SEM studies revealed that films are well adhered to the substrates and no significant failure of the films were observed. Thickness of the films can be controlled by repeating the printing cycle and desired thicknesses can be achieved. Screen printing is a versatile and cheap process which is also quite suitable for continuous application of thick films. Pastes used to deposit films contained large aggregates. Although this situation is related to the powder synthesis conditions, lack of an efficient homogenization technique may lead to such aggregates in the pastes. It is believed that dispersion of powders using high energy ball milling and homogenizing the pastes by roller mills will result in reduction of inhomogenities in the films and degree of agglomeration. Optical studies of the films revealed that visible light transmission of FTO films is highly affected by the agglomerates and resulted in light scattering inside the films decreasing the transparency considerably. In the case of solar cell applications, this light scattering effect is desirable for efficient solar cells causing light trapping and improved photoresponse of cells. However, for future thin film TCO coating demands particles having high transparency and it is obvious that agglomeration has to be prevented.

Dye sensitized solar cells were constructed from FTO nanoparticles after shell coatings of TiO_2 were deposited on the particles from aqueous solutions of titanium precursors as ammonium hexafluorotitanate (AHFT) and titanium tetrachloride.

Resulting structure is a core shell type photoanode. Using these configurations, efficiency of FTO based cells were extensively improved. Efficiency of 1.165 % of FTO based cells were enhanced by AHFT treatment up to 3.79 %. It was observed that efficiency improvement is mostly due to enhanced photovoltage while fill factor and photocurrent remained constant. However, increasing the treatment duration resulted in a strong decrease in photocurrent for cells treated for 45 minutes indicating a suppression of diffusion of electrolyte species and reduction in internal surface area and porosity.

Best efficiency obtained in this work belongs to cells treated with $TiCl_4$. Efficiency of 4.61 % was obtained with enhanced photovoltage and photocurrent values for these cells. Enhancement in photovoltage is attributed to the rise in the fermi level of electrons increasing the chemical potential difference of the cell. In addition to fermi shift, suppression of electronic recombination is believed to be the major factor in the enhancement. Applying a shell coating on FTO particles resulted in an energy barrier layer between photoelectrons and electrolyte, greatly suppressing the recombination reactions. Suppression of back reaction rises voltage, current and fill factor simultaneously as proposed by many authors. Photocurrent density of $TiCl_4$ treated cells, which is around 22.8 mA/cm^2, is competing with the current densities of best TiO_2 films, even higher than TiO_2 cells used in this work. High current is attributed to high electronic mobility of electrons in FTO particles resulting in better electron collection efficiencies and enhanced diffusion rates. However, low value of fill factor around 0.39 indicates still high level of recombination reactions. It is concluded that recombination keeps going through the bare uncoated parts of FTO particles and still inhibits the efficiency. It is believed that applying surface modification techniques achieving full coverage of the surface may lead to further enhanced efficiencies.

In summary, core shell type FTO-TiO_2 photoanodes increased the energy conversion efficiency of solar cells compared to uncoated ones. Although best efficiency obtained in this work is still lower than TiO_2 cells, it seems to be a good strategy to employ outer shell coatings on anodes of cells enhancing the cell parameters. This

type of anodes may also lead to new ways of using different sensitizers of desired electrochemical properties. As the major factor of lower efficiencies of dye sensitized solar cells compared to other pn junction thin films is low photocurrents, high photocurrent obtained in this work is quite promising for higher efficiencies of best TiO_2 cells. It is believed that if more homogeneous shells with optimized thicknesses can be deposited, cell parameters like photovoltage and fill factor may also be further enhanced leading to achieve this goal.

REFERENCES

1. F. Armstrong and K. Blundell, Energy Beyond Oil, Oxford University Press, New York, 2007
2. B. O'Regan and M. Grätzel, A low-cost, high-efficiency solar cell based on dye-sensitized colloidal TiO_2 films. Nature, 1991. 353: p. 737-740
3. M. Gratzel, Conversion of sunlight to electric power by nanocrystalline dye-sensitized solar cells. Journal of Photochemistry and Photobiology A: Chemistry, 2004. 164: p. 3–14
4. E. Suzuki et al., Highly efficient dye-sensitized SnO_2 solar cells having sufficient electron diffusion length. Electrochemistry Communications, 2007. 9: p. 1439–1443
5. K. Tennakone et al., Dye-sensitized solar cells made from nanocrystalline TiO_2 films coated with outer layers of different oxide materials. Coordination Chemistry Reviews, 2004. 248: p. 1277–1281
6. A. Luque and S. Hegedus, Handbook of Photovoltaic Science and Engineering, John Wiley & Sons, England, 2003
7. R. C. Neville, Solar Energy Conversion The Solar Cell 2nd Edition, Elsevier Science B.VA., Amsterdam, 1995
8. A. Goetzberger and J. K. Bernhard, Crystalline Silicon Solar Cells, John Wiley & Sons Ltd., Chichester, 1998
9. T. Markvart and L. Castafier, Solar Cells: Materials, Manufacture and Operation, Elsevier, Amsterdam. 2005
10. B. Sorensen, Renewable Energy: Its physics, engineering, use, environmental impacts, economy and planning aspects 3rd Edition, Elsevier Science, Amsterdam, 2004
11. F. Kreith and Y. Goswami, Handbook of Energy Efficiency and Renewable Energy, Taylor and Francis Group, USA, 2007
12. R Sastrawan, Photovoltaic modules of dye solar cells, PhD dissertation, Freiburg im Breisgau, 2006

13. V. Ramamurthy and K. S. Schanze, Semiconductor Photochemistry and Photophysics, Marcel Dekker Inc., New York, 2003
14. A. Luque and S. Hegedus, Handbook of Photovoltaic Science and Engineering, John Wiley and Sons, Chichester, 2003
15. R. M. Perks et al., Basic materials physics of transparent conducting oxides, Dalton Trans, 2004. p. 2995–3002
16. T. Minami, Transparent conducting oxide semiconductors for transparent electrodes. Semicond. Sci. Technol, 2005. 20: p. 35–44
17. G. J. Exarhos and X. D. Zhou, Discovery-based design of transparent conducting oxide films. Thin Solid Films, 2007. 515: p. 7025–7052
18. M. Gratzel, Conversion of sunlight to electric power by nanocrystalline dye-sensitized solar cells. Journal of Photochemistry and Photobiology A: Chemistry, 2004. 164: p. 3–14
19. U. O. Krasovec et al., Unique TiO_2 paste for high efficiency dye-sensitized solar cells. Solar Energy Materials & SolarCells, 2009. 93: p. 379–381
20. J. R. Durrant et al., Acid versus base peptization of mesoporous nanocrystalline TiO_2 films: functional studies in dye sensitized solar cells. J. Mater. Chem., 2005. 15: p. 412–418
21. A. J. Frank et al., Comparison of dye-sensitized rutile- and anatase-based TiO_2 Solar Cells. J. Phys. Chem. B, 2000. 104: p. 8989-8994
22. J. K. Guo, Preparation and characterizaiton of nanosized TiO_2 powders from aqueous $TiCl_4$ solution. NanoStructured Materials, 1999. 11: p. 1293–1300
23. M. Grätzel et al, Fabrication of thin film dye sensitized solar cells with solar to electric power conversion efficiency over 10%. Thin Solid Films, 2008. 516: p. 4613–4619
24. M. Gratzel et al., Fabrication of screen-printing pastes from TiO_2 powders for dye-sensitised solar cells. Prog. Photovolt: Res. Appl, 2007. 15: p.603–612
25. P. M. Sommeling et al., Influence of a $TiCl_4$ post-treatment on nanocrystalline TiO_2 films in dye-sensitizedsSolar cells. J. Phys. Chem. B, 2006. 110: p. 19191-19197

26. C. A. Grimes et al, Application of highly-ordered TiO2 nanotube-arrays in heterojunction dye-sensitized solar cells. J. Phys. D: Appl. Phys., 2006. 39: p. 2498–2503.
27. P. Schmuki et al., On wafer TiO_2 nanotube-layer formation by anodization of Ti-films on Si. Chemical Physics Letters, 2006. 428: p. 421-425
28. J. J. Lagref, M. K. Nazeeruddin and M. Gratzel, Artificial photosynthesis based on dye-sensitized nanocrystalline TiO_2 solar cells. Inorganica Chimica Acta, 2008. 361: p. 735–745
29. http://www.solaronix.com/products/dyes, Retrieved 11/07/2010
30. G. E. Tulloch, Light and energy dye solar cells for the 21st century. Journal of Photochemistry and Photobiology A: Chemistry, 164: p. 209–219
31. M. Gratzel et al., Highly efficient dye-sensitized solar cells based on carbon black counter electrodes. Journal of The Electrochemical Society, 2006. 153: p. A2255-A2261
32. L.M. Peter et al, Electron transport in the dye sensitized nanocrystalline cell, Physica E, 2002. 14: p. 203 – 209
33. A. J. Frank, N. Kopidakis and J. van de Lagemaat, Electrons in nanostructured TiO_2 solar cells: transport, recombination and photovoltaic properties. Coordination Chemistry Reviews, 2004. 248: p. 1165–1179
34. L.M. Peter, N.W. Duffy, R.L. Wang and K.G.U. Wijayantha, Transport and interfacial transfer of electrons in dye-sensitized nanocrystalline solar cells. Journal of Electroanalytical Chemistry, 2002. 524–525: p. 127–136
35. B. A. Gregg, Interfacial processes in the dye-sensitized solar cell. Coordination Chemistry Reviews, 2004.248: p. 1215–1224
36. E. Fortunato, D. Ginley, H. Hosono and D. C.Paine, Transparent Conducting Oxides for Photovoltaics. MRS Bulletin, 2007. 32: p. 242-247
37. M. Batzill and U. Diebold, The surface and materials science of tin oxide. Progress in Surface Science, 2005. 79: p. 47–154
38. M. Gross, A. Winnacker and P. J. Wellmann, Electrical, optical and morphological properties of nanoparticle indium–tin–oxide layers. Thin Solid Films, 2007. 515: p. 8567–8572

39. J. H. Park, D. J. Byun and J. K. Lee, Electrical and optical properties of fluorine-doped tin oxide (SnOx:F) thin films deposited on PET by using ECR–MOCVD. Journal of electroceramics, 2009. 23: p. 506-511
40. L. C. Costa et al, Microwave shielding of fluorine-doped tin oxide film obtained by spray pyrolysis studied by electrical characterization. Journal of Applied Physics, 2009. 105
41. M. Aguilar et al, Physicochemical characteristics of fluorine doped tin oxide films. J. Phys. D: Appl. Phys., 2006.39: p. 5091–5096
42. E. Llobet et al, Screen-printed nanoparticle tin oxide films for high-yield sensor microsystems. Sensors and Actuators B, 2003. 96: p. 94–104
43. Y. Bai et al., Al_2O_3-coated SnO_2/TiO_2 composite electrode for the dye-sensitized solar cell. Electrochimica Acta, 2005. 50: p. 2583–2589
44. S. Mori et al, Highly efficient dye-sensitized SnO_2 solar cells having sufficient electron diffusion length. Electrochemistry Communications, 2007. 9: p. 1439–1443
45. K. Tennakone, Dye-sensitized solar cells made from nanocrystalline TiO_2 films coated with outer layers of different oxide materials. Coordination Chemistry Reviews, 2004. 248: p. 1277–1281
46. J. Bandara et al., Fabrication of n–pjunction electrodes made of n-type SnO_2 and p-type NiO for control of charge recombination in dye sensitized solar cells. Solar Energy Materials & Solar Cells, 2004. 81: p. 429–437
47. A. Kay and M. Gratzel, Dye-sensitized core-shell nanocrystals: Improved efficiency of mesoporous Ttn oxide electrodes coated with a thin layer of an insulating oxide. Chem. Mater., 2002. 14: p. 2930-2935
48. H. Arakawa et al., Investigations on anodic photocurrent loss processes in dye sensitized solar cells: comparison between nanocrystalline SnO_2 and TiO_2 films. Chemical Physics Letters, 2002.364: p. 297–302
49. N. G. Park et al., Photovoltaic characteristics of dye-sensitized surface-modified nanocrystalline SnO_2 solar cells. Journal of Photochemistry and Photobiology A: Chemistry, 2004. 161: p. 105–110

50. Y. M. Sung et al, Preparation of nanoporous F-doped tin dioxide films for TCO-less dye-sensitized solar cells application. Curr. Appl. Phys., 2009. doi:10.1016/j.cap.2009.11.065
51. S. Chappel and A. Zaban, Nanoporous SnO_2 electrodes for dye-sensitized solar cells: improved cell performance by the synthesis of 18nm SnO_2 colloids. Solar Energy Materials and Solar Cells, 2002. 71: p. 141–152
52. S. Chappel, S. Chen, and A. Zaban, TiO_2-coated nanoporous SnO_2 electrodes for dye-sensitized solar cells. Langmuir, 2002. 18: p. 3336-3342
53. J. R. Durrant et al., Charge transport versus recombination in dye sensitized solar cells employing nanocrystalline TiO_2 and SnO_2 films. J. Phys. Chem. B, 2005. 109: p. 12525-12533
54. N. Park et al., Photovoltaic characteristics of dye-sensitized surface-modified nanocrystalline SnO_2 solar cells. Journal of Photochemistry and Photobiology A: Chemistry, 2004. 161: p. 105–110
55. Y. Diamant, S. G. Chen, O. Melamed, and A. Zaban, Core-Shell nanoporous electrode for dye sensitized solar cells: the effect of the $SrTiO_3$ shell on the electronic properties of the TiO_2 core. J. Phys. Chem. B, 2003. 107: p. 1977-1981
56. J. Chen et al., Dye-sensitized solar cells made from $BaTiO_3$-coated TiO_2 nanoporous electrodes. Journal of Photochemistry and Photobiology A: Chemistry, 2008. 197: p. 260–265
57. J. Zhang and A. Zaban, Efficiency enhancement in dye-sensitized solar cells by in situ passivation of the sensitized nanoporous electrode with Li_2CO_3. Electrochimica Acta, 2008. 53: p. 5670–5674
58. B. Mohagheghi et al., The effect of the post-annealing temperature on the nano-structure and energy band gap of SnO_2 semiconducting oxide nano-particles synthesized by polymerizing–complexing sol–gel method. Physica B, 2008. 403: p. 2431–2437
59. D. Qian et al., High surface area SnO_2 nanoparticles: Synthesis and gas sensing properties. Materials Chemistry and Physics, 2008. 108: p. 232–236

60. A. Hagemeyer et al., High surface area tin oxide. Applied Catalysis A: General, 2007. 317: p. 139–148
61. A. Raj and B. Viswanathan, Effect of surface area, porevolume and particle size of P25 titania on phase transformation of anatase to rutile. Indian Journal of Chemistry, 2009.48A: p. 1378-1382
62. http://www.four-point-probes.com/page19.pdf, Retrieved 27/07/2010